International Journal of
Molecular Sciences

MDPI

Article

IPSC-Derived Neuronal Cultures Carrying the Alzheimer's Disease Associated *TREM2* R47H Variant Enables the Construction of an Aβ-Induced Gene Regulatory Network

Soraia Martins [1], Andreas Müller-Schiffmann [2], Lars Erichsen [1], Martina Bohndorf [1], Wasco Wruck [1], Kristel Sleegers [3,4], Christine Van Broeckhoven [3,4], Carsten Korth [2] and James Adjaye [1,*]

1 Institute for Stem Cell Research and Regenerative Medicine, Medical Faculty, Heinrich-Heine University, 40225 Düsseldorf, Germany; Soraia.Martins@med.uni-duesseldorf.de (S.M.); Lars.Erichsen@med.uni-duesseldorf.de (L.E.); Martina.Bohndorf@med.uni-duesseldorf.de (M.B.); Wasco.Wruck@med.uni-duesseldorf.de (W.W.)
2 Department of Neuropathology, Heinrich-Heine University, 40225 Düsseldorf, Germany; Andreas.Mueller@med.uni-duesseldorf.de (A.M.-S.); ckorth@uni-duesseldorf.de (C.K.)
3 Neurodegenerative Brain Diseases Group, VIB-Center for Molecular Neurology, University of Antwerp, 20610 Antwerp, Belgium; kristel.sleegers@uantwerpen.vib.be (K.S.); christine.vanbroeckhoven@uantwerpen.vib.be (C.V.B.)
4 Department of Biomedical Sciences, University of Antwerp, 20610 Antwerp, Belgium
* Correspondence: james.adjaye@med.uni-duesseldorf.de

Received: 27 May 2020; Accepted: 23 June 2020; Published: 25 June 2020

Abstract: Genes associated with immune response and inflammation have been identified as genetic risk factors for late-onset Alzheimer´s disease (LOAD). The rare R47H variant within triggering receptor expressed on myeloid cells 2 (TREM2) has been shown to increase the risk for developing Alzheimer's disease (AD) 2–3-fold. Here, we report the generation and characterization of a model of late-onset Alzheimer's disease (LOAD) using lymphoblast-derived induced pluripotent stem cells (iPSCs) from patients carrying the TREM2 R47H mutation, as well as from control individuals without dementia. All iPSCs efficiently differentiated into mature neuronal cultures, however AD neuronal cultures showed a distinct gene expression profile. Furthermore, manipulation of the iPSC-derived neuronal cultures with an Aβ-S8C dimer highlighted metabolic pathways, phagosome and immune response as the most perturbed pathways in AD neuronal cultures. Through the construction of an Aβ-induced gene regulatory network, we were able to identify an Aβ signature linked to protein processing in the endoplasmic reticulum (ER), which emphasized ER-stress, as a potential causal role in LOAD. Overall, this study has shown that our AD-iPSC based model can be used for in-depth studies to better understand the molecular mechanisms underlying the etiology of LOAD and provides new opportunities for screening of potential therapeutic targets.

Keywords: late onset Alzheimer's disease; iPSC-derived neuronal cultures; TREM2 R47H; AβS8C dimer

1. Introduction

Currently, there are 47 million people worldwide living with dementia, a number that is estimated to increase to more than 131 million in 2050 [1]. Alzheimer's disease (AD) is a neurodegenerative disease and the most common and devastating cause of dementia, contributing to 60–70% of all cases [2]. AD is clinically characterized by a progressive decline of cognitive functions and, according to the classical

amyloid hypothesis two key molecules have been implicated in AD neuropathology: amyloid-beta (Aß) and the protein TAU [3]. Aß peptides are derived from sequential proteolytic cleavages of the amyloid precursor protein (APP). They form extracellular aggregated deposits known as amyloid plaques. Intracellularly, hyper-phosphorylated TAU forms aggregates composed of twisted filaments known as neurofibrillary tangles (NFTs). As a consequence of the imbalanced crosstalk between Aß and TAU, multiple neuropathological mechanism ensue, such as, synaptic toxicity, mitochondrial dysregulation and microglia-derived inflammatory responses, finally leading to neuronal death [4,5]. Age is the greatest risk factor for AD and it can divided it into early-onset AD (EOAD) when the patients are younger than 65, and late-onset AD (LOAD) when the patients manifest symptoms after the of age 65 [6]. Despite EOAD being responsible for a small minority of all cases, the studies of familiar AD patients (fAD) have revealed important aspects of the genetic factors implicated in the disease, such as the causal mutations in *APP*, *PSEN1* and *PSEN2*. On the other hand, LOAD is a very complex and multifactorial disease where most cases are sporadic with no clear familiar pattern of disease [7,8]. Many genetic risk factors have been implicated in increasing the susceptibility for LOAD, among which is the well establish apolipoprotein E (*APOE).* Individuals carrying one ε4 allele have a 3-fold increased risk of AD while individuals carrying the two ε4 alleles face an approximately 12-fold increased risk of AD [9,10]. More recently genome-wide association studies (GWAS) and large scale sequencing projects have led to the discovery of other genetic variants in more than 40 loci that influence the risk for LOAD [11–16]. These genes are known to be involved in biological pathways such as cholesterol metabolism, APP metabolism, MAPT metabolism, cytoskeleton and axon development, immune response and endocytosis/vesicle-mediated transport and epigenetics [17,18]. As a more direct link between immune responses and AD, especially microglia-related genes with an increased risk for developing LOAD were identified by high-throughput sequencing technologies [19,20]. One of multiple genetic risk variants identified in these studies is the rare p.Arg47His (R47H) variant within triggering receptor expressed on myeloid cells 2 (*TREM2*), which has been shown to increase the risk of developing AD by 2–3-fold in several European and North American populations [19–24].

TREM2 is a cell surface receptor of the immunoglobulin superfamily expressed on various cells of the myeloid linage including CNS microglia, bone osteoclasts, alveolar and peritoneal macrophages [25] According to neuropathology studies in AD patients, animal models and in vitro studies, the *TREM2* R47H variant induces a partial loss of function of TREM2, compromising microglia function and thus contributing to the development of AD. TREM2 deficiency in AD mouse models and patients carrying the R47H variant showed decreased clustering of microglia around the plaques, thereby facilitating the build-up of Aβ plaques and injury to adjacent neurons [26–29]. Recent data have shown that cells expressing the R47H variant displayed impaired TREM2-Aβ binding and altered TREM2 intracellular distribution and degradation, thus providing a potential mechanism by which *TREM2* R47H mutation increases the risk for LOAD [30,31]. The adoption of induced pluripotent stem cells (iPSCs) technology provides a platform to derive a reliable human disease model for better understanding the effect of risk factors in neurons derived from primary cells of affected patients. iPSC modeling of AD has provided an important proof-of-principle regarding the utility of such cells for a better understanding of the molecular mechanisms associated with the etiology of AD. So far, a number of the human iPSC-based AD models have concentrated on using iPSCs derived from EOAD or LOAD patients with unidentified mutations [32–38].

Here, we report for the first time the generation and characterization of a model of LOAD using lymphoblast-derived iPSCs from patients harboring the R47H mutation in *TREM2*, as well as from control individuals without dementia. To date gene regulatory networks governing LOAD have been generated using human AD brain biopsies. In our current study, we have shown the feasibility of using an iPSC-based approach to derive biologically meaningful pathways and an Aβ-induced regulatory network from neuronal cultures that mirrors some of the pathways that have been identified by the LOAD brain biopsies, namely immune response, phagocytosis and unfolded protein response pathways [39]. Our study thus demonstrates that AD iPSC-derived neuronal cultures can be used for

in depth studies to understand the molecular mechanisms underlying the onset of Alzheimer's disease and for screening of potential therapeutic targets.

2. Results

2.1. Ipscs Efficiently Differentiate into a Functional Neuronal Culture

iPSCs derived from lymphoblasts from two LOAD patients carrying the *TREM2* R47H risk variant (AD2-2 and AD2-4), as well as aged-matched control individuals without dementia (CON8 and CON9) were used for this study [40–43]. The summary of the characteristics of the iPSC lines used in this study as well as their APOE status are shown in Table 1.

Table 1. Summary of the healthy controls and Alzheimer's disease (AD) induced pluripotent stem cell (iPSC) lines used in this study.

iPSCs Name	Status	AD Risk Variant	Age	Age at Onset	Gender	APOE Genotype	Reference
CON8	Control individual	Control	69	-	M	3/4	[43]
CON9	Control individual	Control	75	-	F	3/3	[40]
AD-2-2	AD patient	TREM2 p.R47H heterozygous	65	60	M	4/4	[42]
AD-2-4	AD patient	TREM2 p.R47H heterozygous	67	64	F	2/4	[41]

It has been suggested that GABAergic neurotransmission plays a very important role in AD pathogenesis such as Aβ toxicity, hyperphosphorylation of TAU and the APOE effect [44–46]. In light of this information, we modified a previously established embryoid body-based protocol [47] to generate iPSC-derived neuronal cultures enriched in GABAergic interneurons. Figure 1A shows the timeline schematic for the protocol in which all iPSC lines were successfully differentiated into neuronal networks enriched in GABAergic interneurons within a course of 80 days (Figure S1). To qualitatively characterize the progression of differentiation, we performed immunostaining for various markers during the differentiation process. Neural rosettes expressed the progenitor markers PAX6 and Nestin (Figure 1B) and after being selected and grown as neurospheres for 7 days, the progenitor cells ($SOX1^+$) acquired predominantly a forebrain identity due to the expression of the medial ganglionic eminence (MGE) transcription factor NKX2.1 (Figure 1C), in addition to the telencephalic transcription factor FOXG1 (Figure 1D). After maturation, the neural cultures were composed of $GFAP^+$ glia cells and neurons expressing the pan-neuronal markers Tubulin Beta-III and MAP2 (Figure 1E). Neurons differentiated for 80 days expressed the maturation markers Synapsin I (SYN1) and neurofilaments (SMI-32; Figure 1F), as well as the neurotransmitter, GABA (Figure 1G). In order to assess the maturation status of the neuronal cultures, we performed RNA sequencing to analyze the transcriptome profile at day 80. Figure 1H shows a heat map of Pearson correlation analysis for key maturation neuronal markers together with the glia markers OLIG2 and GFAP in the iPSC-derived neuronal cultures compared to commercially bought RNA from fetal, adult and AD brain. All iPSC-derived neuronal cultures expressed similar levels of dopaminergic and serotonergic markers and higher levels of GABAergic interneuron markers. To complement and independently confirm these expression data, quantitative real-time PCR (qRT-PCR) analysis was carried out to evaluate the expression levels of GABAergic interneuron markers *PV, SOM, CALB2, GAD67* and *GAD65* (Figure S1). Despite the variability of expression levels of the different markers, we observed that the iPSC-derived neuronal cultures might be composed mostly of somatostain (SST) and calretinin (CALB2) subtypes of GABA

interneurons. Moreover, due to the low expression level observed for *TREM2* when compared with the commercially bought fetal, adult and AD brain RNA, qRT-PCR was performed for all iPSC-derived neuronal cultures. *TREM2* is expressed in all lines but however significantly upregulated in AD2-2 (Figure 1I). Taken together, we proposed (i) that the presence of the *TREM2* R47H variant in the AD2-2 and AD2-4 lines has no significant effect on the neuronal differentiation capacity when compared to the control lines CON8 and CON9, (ii) though we did not analyze our neuronal cultures for the presence of microglia, the mixed neuronal culture might probably harbor these.

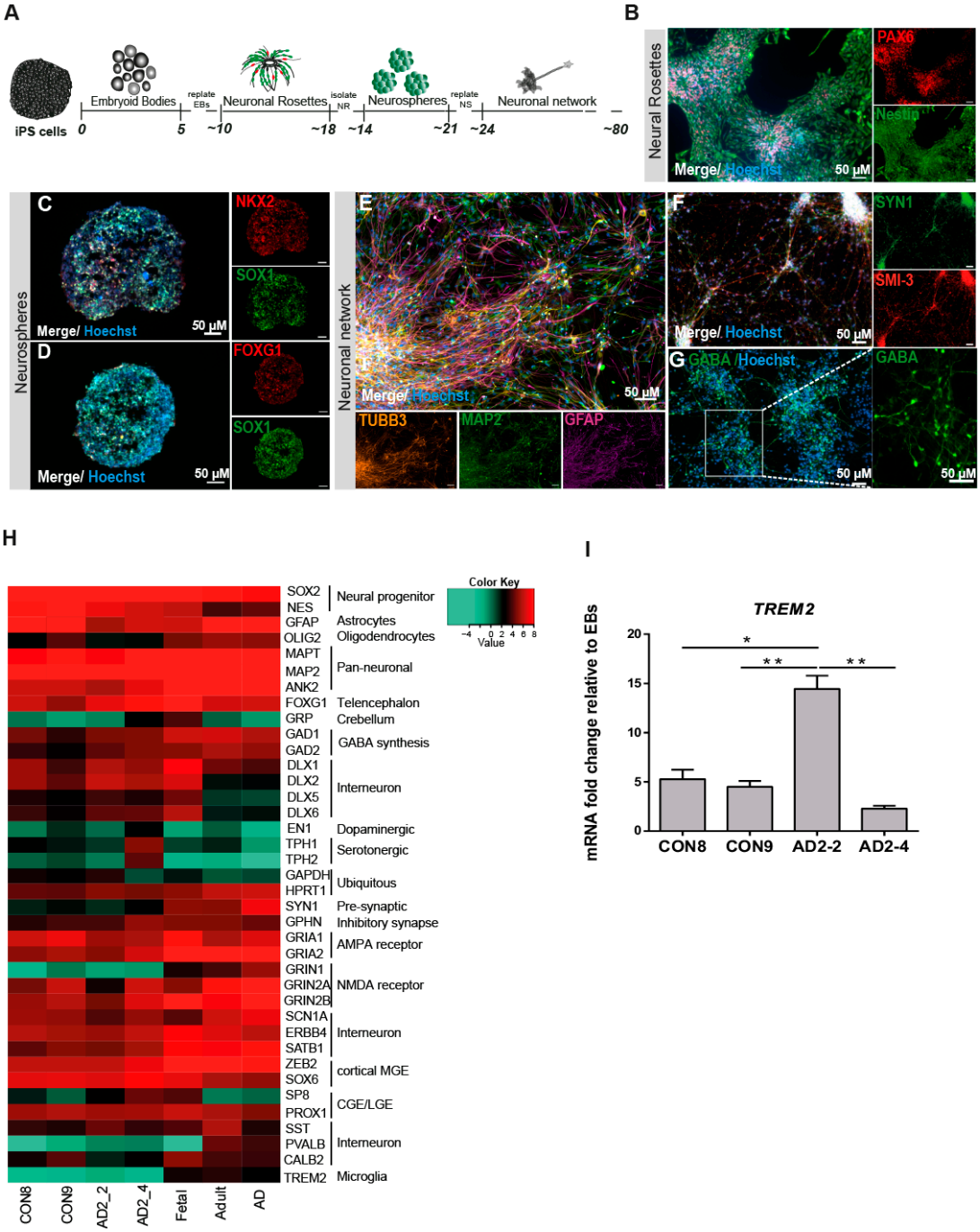

Figure 1. Differentiation and characterization of iPSC-derived neuronal cultures. (**A**) Scheme illustrating the main stages of the differentiation protocol for generating iPSC-derived neuronal network enriched in GABAergic interneurons. (B-G) Representative immunocytochemistry images of (**B**) neural rosettes

expressing the progenitor markers PAX6 (red) and Nestin (green), (**C**) neurosphere expressing the progenitor marker SOX1 (green) and the MGE marker NKX2.1 (red), (**D**) neurosphere expressing the progenitor marker SOX1 (green) and the forebrain marker FOXG1 (red), (**E**) neuronal network expressing the pan-neuronal markers TUBB3 (orange) and MAP2 (green) as well as GFAP (magenta), (**F**) neural maturation markers SYN1 (green) and SMI-3 (red) and (**G**) interneurons expressing the neurotransmitter GABA (green). Nuclei are stained with Hoechst. Scale bar, 50 µM. (**H**) Heatmap of Pearson correlation analysis of RNA-seq data from neural differentiation of control (CON8 and CON9) and AD lines (AD2_2 and AD2 _4) and commercially bought RNA from fetal, adult and AD brain for neural progenitor, early neuronal and mature dopaminergic, serotonergic, GABAergic interneuronal markers and glia markers. (**I**) Relative gene expression of TREM2 in iPSC-derived GABAergic interneurons network from control and AD lines shown as fold change relative to embryoid bodies (EBs). * $p < 0.05$, ** $p < 0.01$, one-way ANOVA, followed by Tukey´s multiple comparisons test. Data are presented as mean ± SEM from three independent experiments.

2.2. The AD Neuronal Network Shows a Distinct Gene Expression Associated with Metabolism and Immune-Related Pathways

To obtain an overview of the transcriptome changes between the AD (AD2-2 and AD2-4) and the control (CON8 and CON9) neuronal cultures, we screened for differentially expressed genes (DEGs). Employing RNA-seq, we identified 4990 genes exclusively expressed in the AD neuronal cultures (Figure 2A). BiNGO was used to perform gene ontology (GO) term enrichment analysis of the 4990 genes, the results are illustrated as a tree-like structure (Figure 2B, Table S1). In depth analyses of the cellular component identified significant enrichment associated with membrane and extracellular space. Regarding biological processes, these genes were significantly enriched in processes related to the response to the stimulus and transport. Moreover, molecular functions such as signal transducer activity, receptor activity and transporter activity, including ion membrane transporter activity and channel activity were significantly enriched. Kyoto Encyclopedia of Genes and Genomes (KEGG) pathway analysis revealed metabolic pathways, which include drug metabolism—cytochrome P450, retinol metabolism and steroid hormone biosynthesis together with a neuroactive ligand–receptor interactor (Figure 1C). As it has been shown that TREM2 regulates innate immunity in AD [48], we additionally analyzed GO terms for biological processes of immune-related genes within the 4990 gene set. Remarkably, 14 significantly enriched terms associated with the regulation of innate and adaptive immune response were identified (Figure 2D). Overall, these data may suggest that AD neuronal cultures exhibit alterations in key signaling pathways related to metabolism and the immune system.

2.3. Characterization of AD Hallmarks in CON and AD Neuronal Cultures

Numerous evidence support the notion that the small oligomers of $A\beta_{42}$ are intricately associated with the amyloid cascade [49,50]. However, recent studies have shown that Aβ dimers, abundantly detected in brains of AD patients, are sufficient to account for neurotoxicity and initiating the amyloid cascade [51–54]. Here, we aimed at investigating the effects of the *TREM2* R47H mutation in Aβ production as well as the response of CON and AD iPSC-derived neuronal cultures to stimulations with the well described Aβ-S8C dimer [55–57]. After 4 months of differentiation, neurospheres were dissociated into single cells and differentiated for a further 6 weeks. Aβ levels were measured and the neuronal cultures were stimulated with 500 nM of the Aβ-S8C dimer for 72 h (Figure 3A). Conditioned media from the non-stimulated CON and AD lines were analyzed for comparative $A\beta_{40}$ and $A\beta_{42}$ levels employing ELISA. Interestingly, neurons derived from the AD iPSCs lines (AD2-2 and AD2-4) and the CON iPSCs lines (CON8 and CON9) secreted Aβ with similar $A\beta_{42}$ ratio (Figure 3B-D). We further performed Western blot analysis to evaluate the levels of TAU phosphorylation at Ser202/Thr205 (AT8 epitope), total TAU and total APP after stimulation with the Aβ-S8C dimer (Figure 3E). Although phosphorylation of TAU was found in all neuronal cultures, no significant differences in the expression levels of total TAU (Figure 3F) and phosphorylated TAU (Figure 3G) were observed between AD and

CON neuronal cultures after treatment with the Aβ-S8C dimer. Surprisingly, the results revealed that stimulation with the Aβ-S8C dimer induced a modest and uniform increase in the expression levels of APP in all CON and AD neuronal cultures (Figure 3H). To focus on the effect of the Aβ-S8C dimer, we quantified APP levels in pooled samples, and this revealed significantly increased APP expression (Figure 3I). Taken together, these results confirm that the neuronal cultures (CON8 and AD) secrete Aβ and although no significant differences in the expression of total and phosphorylated TAU were observed, APP expression was significantly elevated after Aβ-S8C dimer stimulation. We therefore conclude that the CON and the AD iPSC-derived neuronal cultures were capable of recapitulating in vitro the hallmarks of AD-like cellular pathology.

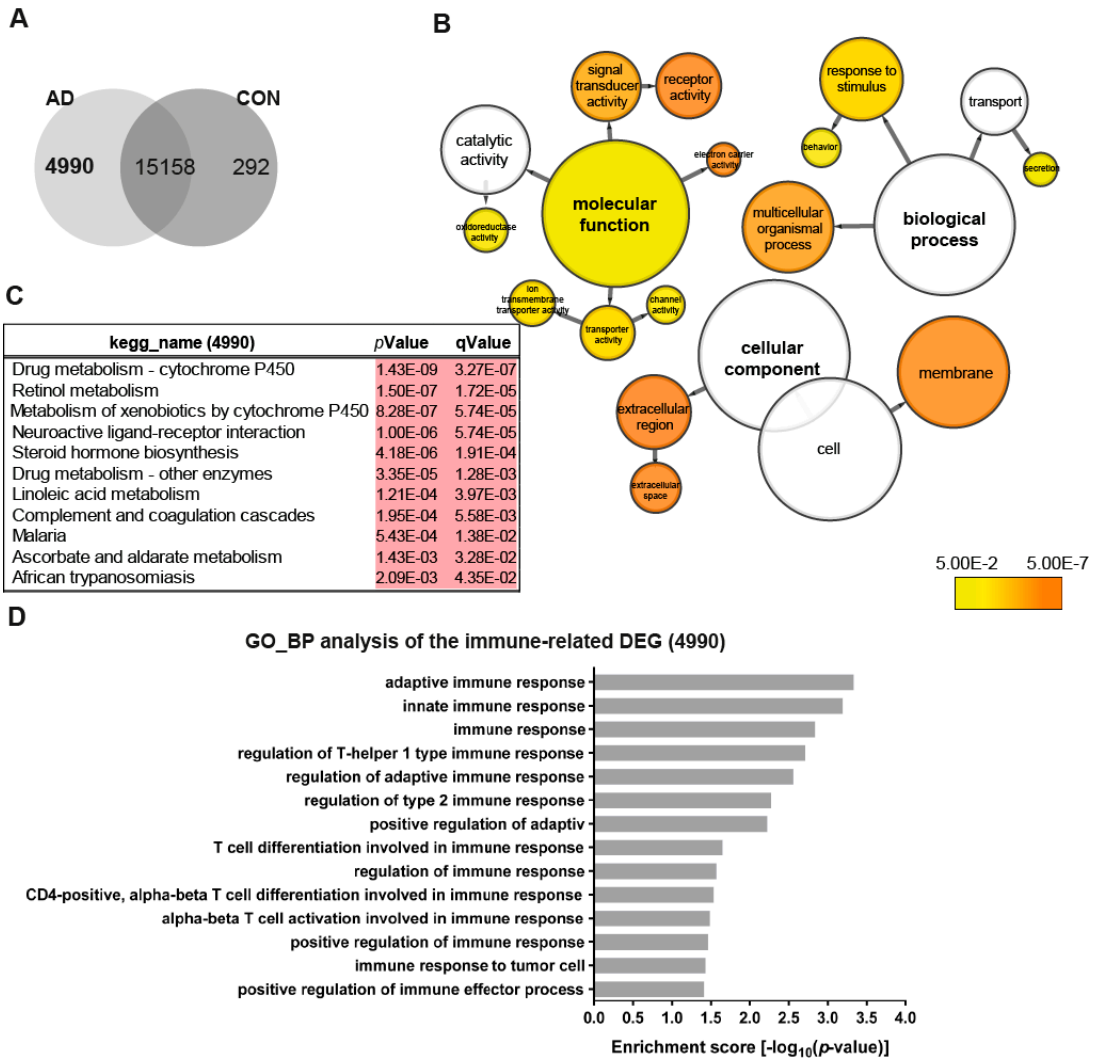

Figure 2. Distinct gene expression profiles associated with AD neuronal networks. (**A**) Venn diagram illustrating genes exclusively expressed in the AD neural network (4990), the control (CON) network (292) or common between both (intersection -15158) (detection p-value < 0.05). (**B**) BiNGO analysis of the differentially expressed genes (DEGs; 4990) exclusively expressed in the TREM2 neuronal network (4990). The orange color of the circles correspond to the level of significance of the over-represented gene ontology (GO) category and the size of the circles is proportional to the number of genes in the category (p-value < 0.05). (**C**) Kyoto Encyclopedia of Genes and Genomes (KEGG) pathway analysis of the genes exclusively expressed in the AD neuronal network (4990). (**D**) Significantly enriched gene ontology (GO) terms (biological processes) of the genes exclusively expressed in the AD neuronal network (4990) associated with immune system processes (p-value < 0.05).

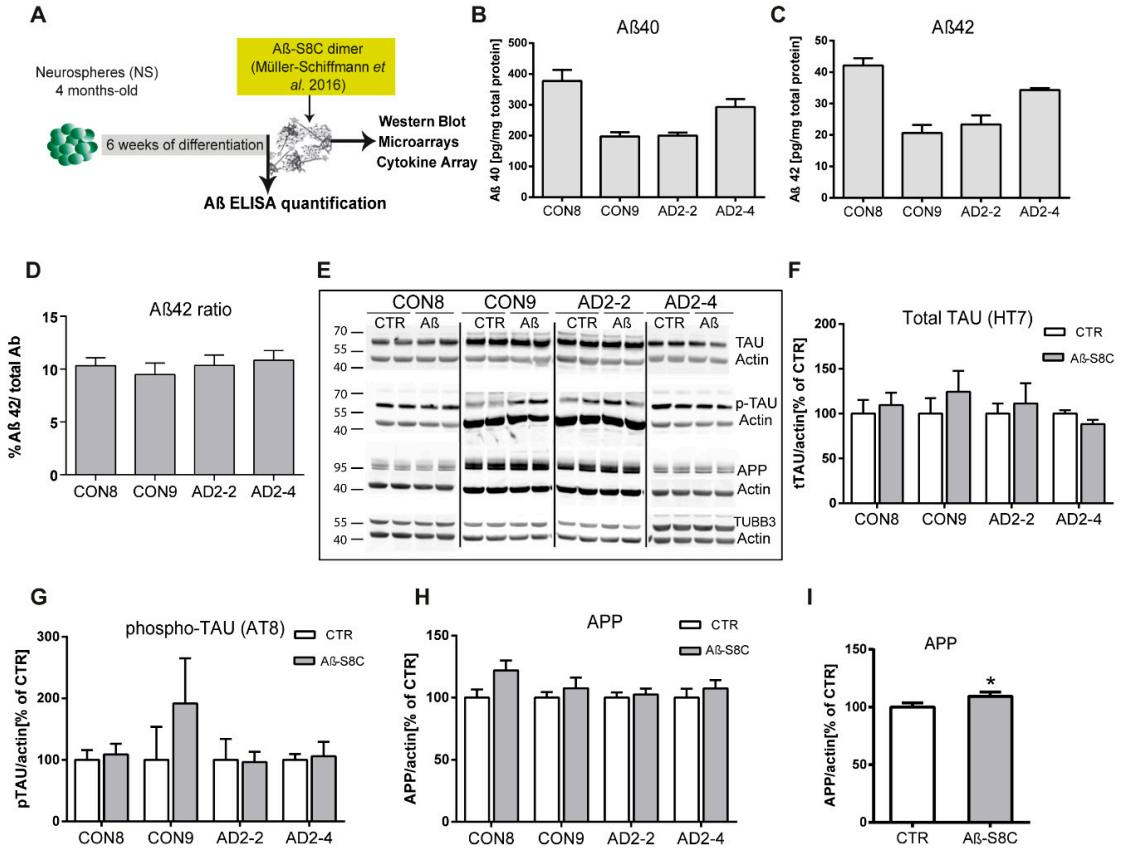

Figure 3. Stimulation of iPSC-derived neuronal cultures with the Aβ-S8C dimer. (**A**) Scheme illustrating the approach. Neurospheres were maintained for 4 months in culture, dissociated into single cells, differentiated for 6 weeks then stimulated with 500 nM of Aβ-S8C dimer for 72 h. Western blotting, microarrays and cytokine arrays were performed. (B-D) ELISA quantification of (**B**) total Aβ40, (**C**) total Aβ42 levels and (**D**) Aβ42/Aβ40+42 ratio from media collected from the interneuronal network and normalized to the total protein content. All data are presented as mean ± SEM from six independent experiments. (**E**) Representative Western blot images of endogenous TAU, phosphorylated TAU (Ser 202 and Thr 205), APP and the neural differentiation marker βIII-Tubulin after stimulation with 500 nM of the Aβ-S8C dimer. β-ACTIN was used as a loading control. (F-H) Quantification of (**F**) total TAU, (**G**) phosphorylated TAU and (**H**) APP levels. Results are normalized against β-ACTIN and shown as a percentage of control (CTR). All data are presented as mean ± SEM from 3 independent experiments. (**I**). Effect of the Aβ-S8C dimer on APP levels in iPSCs derived neuronal network (CON8, CON9, AD2-2 and AD2-4) compared to control. Data are presented as mean ± SEM from 3 independent experiments from 4 biological replicates. * $p < 0.05$, one-tail t-test versus control.

2.4. The Aβ-S8C Dimer Induces Metabolic Dysregulation in AD Neuronal Cultures

To assess the impact of the Aβ-S8C dimer on the gene expression profiles of CON and AD iPSC-derived neuronal cultures, we performed transcriptome analysis of CON8 and AD2-4 iPSC-derived neuronal cultures before and post stimulation with the Aβ-S8C dimer. This analysis identified differential expressed genes (DEGs) between the control and Aβ-S8C dimer treatment. Hierarchical cluster analysis revealed a clear separation of CON8 and AD-TREM2-4 iPSC-derived neuronal cultures (Figure 4A). Remarkably, CON8_Aβ clustered separately from AD2-4_Aβ, therefore implying that genetic background effects were more pronounced than the response elicited by the Aβ-S8C dimer.

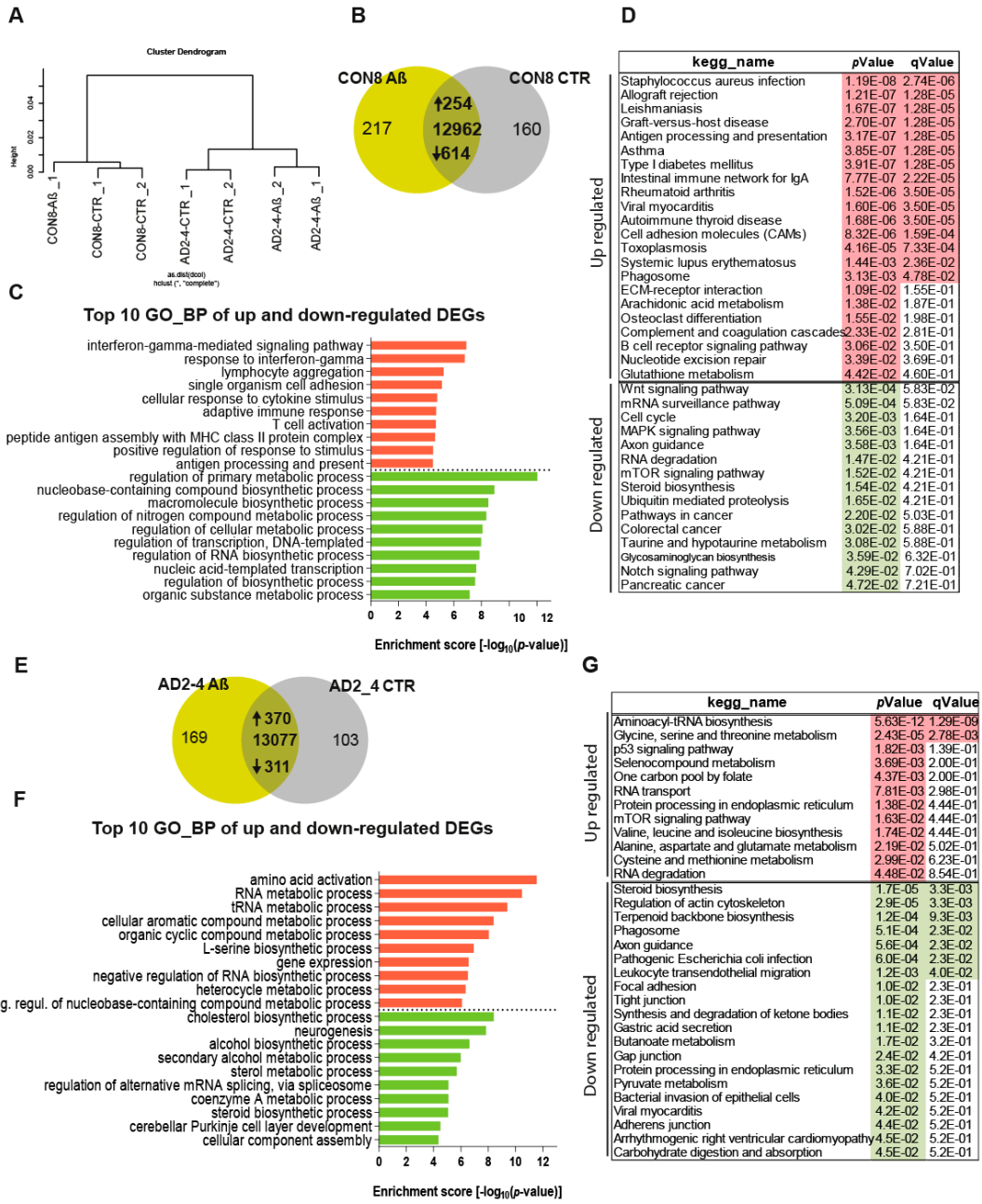

kegg_name	pValue	qValue
Staphylococcus aureus infection	1.19E-08	2.74E-06
Allograft rejection	1.21E-07	1.28E-05
Leishmaniasis	1.67E-07	1.28E-05
Graft-versus-host disease	2.70E-07	1.28E-05
Antigen processing and presentation	3.17E-07	1.28E-05
Asthma	3.85E-07	1.28E-05
Type I diabetes mellitus	3.91E-07	1.28E-05
Intestinal immune network for IgA	7.77E-07	2.22E-05
Rheumatoid arthritis	1.52E-06	3.50E-05
Viral myocarditis	1.60E-06	3.50E-05
Autoimmune thyroid disease	1.68E-06	3.50E-05
Cell adhesion molecules (CAMs)	8.32E-06	1.59E-04
Toxoplasmosis	4.16E-05	7.33E-04
Systemic lupus erythematosus	1.44E-03	2.36E-02
Phagosome	3.13E-03	4.78E-02
ECM-receptor interaction	1.09E-02	1.55E-01
Arachidonic acid metabolism	1.38E-02	1.87E-01
Osteoclast differentiation	1.55E-02	1.98E-01
Complement and coagulation cascades	2.33E-02	2.81E-01
B cell receptor signaling pathway	3.06E-02	3.50E-01
Nucleotide excision repair	3.39E-02	3.69E-01
Glutathione metabolism	4.42E-02	4.60E-01
Wnt signaling pathway	3.13E-04	5.83E-02
mRNA surveillance pathway	5.09E-04	5.83E-02
Cell cycle	3.20E-03	1.64E-01
MAPK signaling pathway	3.56E-03	1.64E-01
Axon guidance	3.58E-03	1.64E-01
RNA degradation	1.47E-02	4.21E-01
mTOR signaling pathway	1.52E-02	4.21E-01
Steroid biosynthesis	1.54E-02	4.21E-01
Ubiquitin mediated proteolysis	1.65E-02	4.21E-01
Pathways in cancer	2.20E-02	5.03E-01
Colorectal cancer	3.02E-02	5.88E-01
Taurine and hypotaurine metabolism	3.08E-02	5.88E-01
Glycosaminoglycan biosynthesis	3.59E-02	6.32E-01
Notch signaling pathway	4.29E-02	7.02E-01
Pancreatic cancer	4.72E-02	7.21E-01

kegg_name	pValue	qValue
Aminoacyl-tRNA biosynthesis	5.63E-12	1.29E-09
Glycine, serine and threonine metabolism	2.43E-05	2.78E-03
p53 signaling pathway	1.82E-03	1.39E-01
Selenocompound metabolism	3.69E-03	2.00E-01
One carbon pool by folate	4.37E-03	2.00E-01
RNA transport	7.81E-03	2.98E-01
Protein processing in endoplasmic reticulum	1.38E-02	4.44E-01
mTOR signaling pathway	1.63E-02	4.44E-01
Valine, leucine and isoleucine biosynthesis	1.74E-02	4.44E-01
Alanine, aspartate and glutamate metabolism	2.19E-02	5.02E-01
Cysteine and methionine metabolism	2.99E-02	6.23E-01
RNA degradation	4.48E-02	8.54E-01
Steroid biosynthesis	1.7E-05	3.3E-03
Regulation of actin cytoskeleton	2.9E-05	3.3E-03
Terpenoid backbone biosynthesis	1.2E-04	9.3E-03
Phagosome	5.1E-04	2.3E-02
Axon guidance	5.6E-04	2.3E-02
Pathogenic Escherichia coli infection	6.0E-04	2.3E-02
Leukocyte transendothelial migration	1.2E-03	4.0E-02
Focal adhesion	1.0E-02	2.3E-01
Tight junction	1.0E-02	2.3E-01
Synthesis and degradation of ketone bodies	1.1E-02	2.3E-01
Gastric acid secretion	1.1E-02	2.3E-01
Butanoate metabolism	1.7E-02	3.2E-01
Gap junction	2.4E-02	4.2E-01
Protein processing in endoplasmic reticulum	3.3E-02	5.2E-01
Pyruvate metabolism	3.6E-02	5.2E-01
Bacterial invasion of epithelial cells	4.0E-02	5.2E-01
Viral myocarditis	4.2E-02	5.2E-01
Adherens junction	4.4E-02	5.2E-01
Arrhythmogenic right ventricular cardiomyopathy	4.5E-02	5.2E-01
Carbohydrate digestion and absorption	4.5E-02	5.2E-01

Figure 4. Gene expression profiles of the CON8 and AD neural cultures stimulated with the Aβ-S8C dimer. (**A**) Dendrogram obtained by hierarchical cluster analysis of microarray-based (Affymetrix) gene expression data for CON8 and AD2-4 stimulated with the Aβ-S8C peptide. Transcriptomes of CON8_CTR cluster with CON8_ Aβ while those of the AD2-4_CTR cluster separately with TREM2-4_ Aβ. (**B**) Venn diagram showing genes expressed only in the CON8 neural network subjected to Aβ-S8C peptide stimulation (green), the control condition (grey) and common to both conditions (intersection; detection p value < 0.05). (**C**) Top 10 significantly enriched gene ontology (GO) terms for biological processes of DEGs upregulated (254-red) and downregulated (614-green) subjected to Aβ-S8C peptide stimulation in CON8 neuronal cultures (p-value < 0.05). (**D**) KEGG enrichment analysis of up- and downregulated DEGs (p-value < 0.05). (**E**) Venn diagram showing genes expressed only in the AD2_4 neuronal culture when stimulated with the Aβ-S8C peptide (green), the control condition (grey) and common to both conditions (intersection; detection p value < 0.05). (**F**) Top 10 significantly enriched gene ontology (GO) terms for biological processes of DEGs upregulated (370-red) and downregulated (311-green) subjected to Aβ-S8C peptide stimulation in the AD2_4 neuronal cultures (p-value < 0.05). (**G**) KEGG enrichment analysis of up- and downregulated DEGs (p-value < 0.05).

Evaluation of DEGs in CON8 neuronal cultures before and after stimulation with the Aβ-S8C dimer identified 868 genes (Figure 4B), 254 were upregulated and 614 downregulated (Table S1). Figure 4C shows the related Top10 GO BP (biological processes) terms. Upregulated genes in CON8_Aβ were significantly enriched for GO terms such as interferon-gamma-mediated signaling pathway and cellular response to cytokine stimulus. In contrast, the downregulated genes in CON8_Aβ in comparison to control were associated with the GO terms, regulation of primary metabolic processes and regulation of RNA biosynthetic process. In agreement with the GO analysis, KEGG pathway analysis for the same set of genes revealed the upregulated genes in CON8_ Aβ to be associated in pathways related to inflammatory responses, for example, *Staphylococcus aureus* infection and antigen processing and presentation. In addition, CON8_Aβ also showed upregulation of the phagosome pathway, while Wnt signaling pathway and axon guidance were among the downregulated KEGG pathways (Figure 4D, Table S1).

Focusing on AD neuronal cultures, 681 DEGs were identified when comparing Aβ-S8C dimer stimulated and non-stimulated AD2-4 neuronal cultures (Figure 4F), of these 370 were upregulated and 311 downregulated (Table S2). Figure 4F lists the Top 10 GO BP terms. The upregulated genes in AD2-4_Aβ were significantly enriched for amino acid activation and RNA metabolic process. In contrast, the downregulated genes were associated amongst others with cholesterol biosynthetic process and neurogenesis. KEGG pathway analysis revealed upregulation of pathways such as glycine, serine and threonine metabolism, p53 signaling pathway and mTOR signaling pathway. Surprisingly, in contrast to CON8_Aβ, AD2-4 neuronal cultures stimulated with Aβ-S8C dimers showed down-regulation of the phagosome pathway (Figure 4G, Table S2). Taken together, these results imply that the AD2-4 neuronal cultures respond in a unique way to Aβ-S8C dimer stimulation, namely a metabolic dysregulation in contrast to an inflammatory response, which could be observed in the CON8 neuronal cultures.

2.5. Aβ-S8C Dimer Stimulation of the AD Neuronal Culture Revealed Indications of Impaired Phagocytosis-Related Pathway

TREM2 is crucial for regulating phagocytosis in microglia and the effect in phagocytosis by the AD-associated *TREM2* mutations have recently been a focus of studies [58–63]. As described above, phagocytosis appeared as a significantly upregulated pathway in CON8 but was downregulated in AD2-4 neuronal cultures after Aβ stimulation. We then analyzed differential expression of genes associated with this pathway. Figure 5A depicts the KEGG annotated phagosome pathway with upregulated genes in CON8_Aβ (red) and those downregulated in AD2-4_Aβ (green). After stimulation with the Aβ-S8C dimer, CON8 induced upregulation *of HLA-DMA, HLA-DMB. HLA-DOA, HLA-DPB1, HLA-DQA1, HLA-DQB1, HLA-DRB1* and *HLA-F*, all genes associated with the Major Histocompatibility complex II (MHCII). In contrast to the AD2-4 non-stimulated cultures, stimulation with the Aβ-S8C dimer induced down-regulation of *TUBB4A, TUBB4B, DYNC1H1, LAMP2, ATP6V1A, ACTB, THBS1, CALR* and *TUBBA1C*. Table S3 shows the relative mRNA expression, from which the expression of *CALR, DYNC1H, LAMP2, HLA-DOA* and *HLA-DQB1* was confirmed by RT-PCR (Figure 5B). Taken together, these results suggest that neuronal cultures harboring the *TREM2* R47H variant but not controls likely undergo an impaired phagocytosis response in the presence of the Aβ-S8C dimer.

2.6. AD Neuronal Cultures Show a Compromised Inflammatory Response-Related Gene Expression Pattern upon Stimulation with the Aβ-S8C Dimer

Based on the fact that dysregulated cytokine production from microglia, astrocytes and neurons are associated with the development of AD [64], we analyzed the cytokine expression profile as well as the secretion profile from the AD neuronal cultures after stimulation with the Aβ-S8C dimer. Employing microarray-based global gene expression data, a heatmap-based analysis of 100 key cytokines (extracted from the Proteome Profiler Human XL Cytokine Array, R&D systems) revealed that stimulation with the Aβ-S8C dimer induced transcriptional changes in a subset of these genes in AD-TREM2-4 (Figure 6A). Interestingly, the AD2-2 neuronal culture showed down-regulation of

cytokines, chemokines and acute phase genes such as *IL1RL1, IL13, IL15, IL16, IL27, IL32, CXCL10, CXCL11, TFRC, SERPINE1, C5, THBS1, RLN2, SPP1, EGF, LIF, GC, BSG, MPO, CST3, FLT3LG* and *CCL20*. Surprisingly, only *IGFBP2, RBP4, VEGFA, CXCL5, IL19* and *TDGF1* had higher expression levels after Aβ-S8C dimer stimulation when compared to the control samples. We next aimed at determining if stimulation with the Aβ-S8C dimer could also alter the secretion of cytokines and chemokines in the AD neuronal cultures. To this end, we collected the cell culture supernatants from the AD2-2 and AD2-4 neuronal cultures 72 h post stimulation with the Aβ-S8C dimer and from non-stimulated controls. Thereafter, we carried out secretome analysis employing the proteome profiler cytokine array (Figure 6B). In agreement with the previous results, the level of secretion of all cytokines and chemokines decreased after Aβ-S8C dimer stimulation when compared to control (Figure 6C), with the exception of ICAM-1, MIF and SerpinE1. Taken together, these results might imply that AD neuronal cultures compromise the efficient activation of the inflammasome pathway in response to Aβ-S8C dimer stimulation.

2.7. A Protein–Protein Interaction (PPI) Network Identifies an AD-Depended Aβ-S8C Signature

To gain insights into a probable gene expression signature triggered by the Aβ-S8C dimer in LOAD, we focused on genes exclusively expressed in the AD neuronal culture after stimulation with the Aβ-S8C dimer. A Venn diagram analysis revealed that most (12687) genes were expressed in common between CON and AD with and without Aβ-S8C dimer stimulation (Figure 7A, Table S4). However, 95 genes were exclusively expressed in AD neuronal cultures stimulated with Aβ-S8C dimer. GO analysis (Figure 7B) unveiled several terms related to neuron and immune-system related processes including stimulatory C-type lectin receptor signaling pathway as most significant. Pathway analysis of the 95 AD Aβ-S8C genes (Figure 7C) revealed neuroactive ligand-receptor interaction as the most significant pathway and metabolic pathways with the higher number of genes. The 95 genes were further analyzed in a protein–protein interaction network (PPI) based on interactions from the BioGrid database resulting in a network containing APP and a big hub centered around *HSPA5*, which encodes the endoplasmic reticulum chaperone BiP (Figure 7D). HSPA5 has been reported to control the activation of the unfolding protein response (UPR), a pro-survival pathway in response to ER stress caused by misfolded proteins. Since there is evidence that the ER stress response, namely the UPR plays a role in the pathogenesis of AD [65], we took a deeper look into the GO terms related to ER after Aβ-S8C dimer stimulation (Table S2, highlighted in yellow). We observed that the Aβ-S8C dimer triggered an ER stress response, which elevated the expression of *ATF3* and *DDIT* in both CON and AD. Interestingly, the ER stress response was more prominent in the AD neuronal cultures, where several genes from the UPR were upregulated (*XBP1, AT4, PUMA* and *HERPUD1*) in contrast to *HSPA5* and *CALR*, which were downregulated (Figure 8, Table S5). These results highlighted the unique response triggered by the Aβ-S8C dimer in the AD neuronal cultures. By generating a PPI network we were able to link the Aβ-S8C signature genes to ER-stress, namely the activation of UPR.

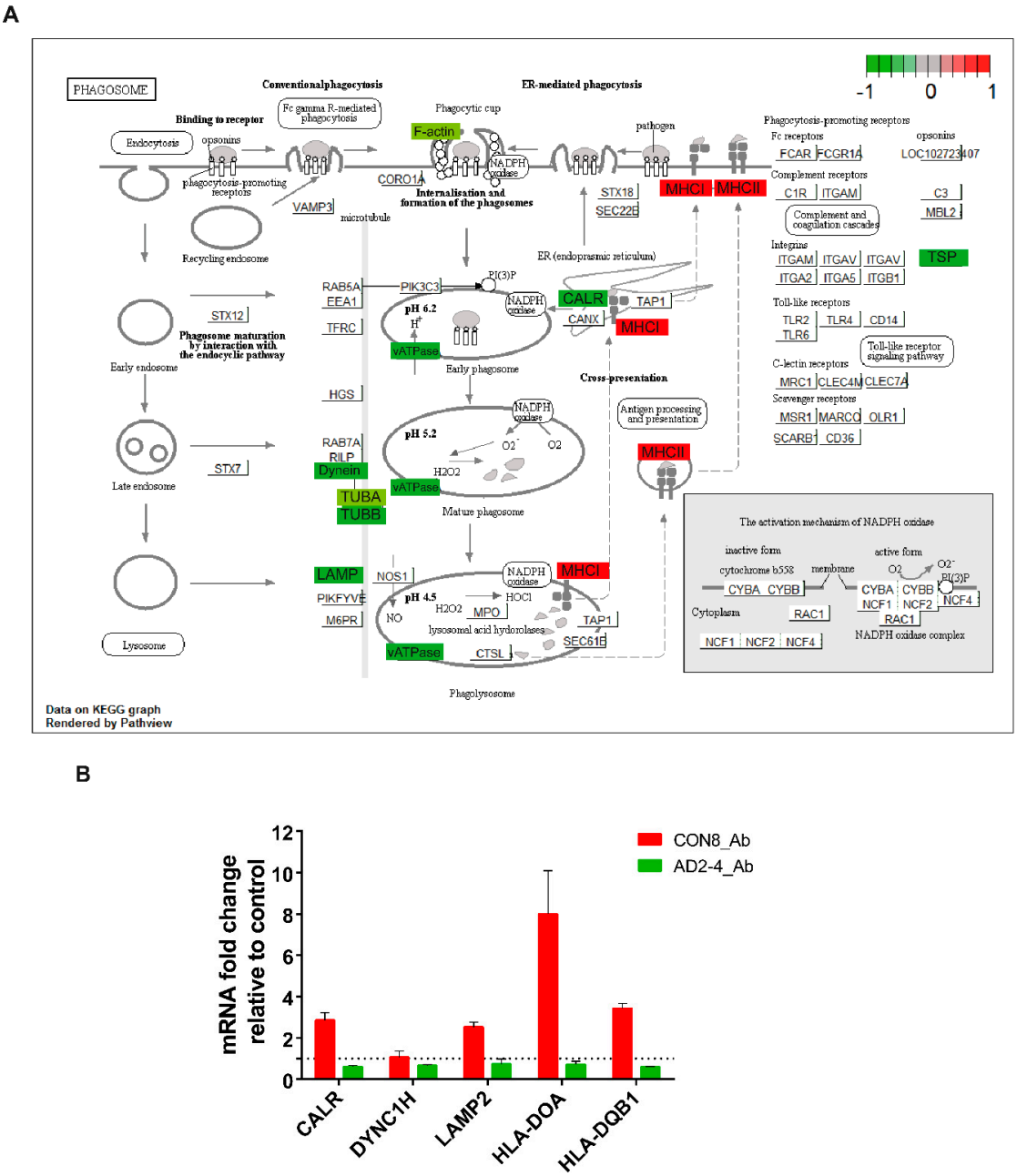

Figure 5. Representation of the KEGG phagosome pathway. (**A**) Upregulated DEGs genes in response to Aβ-S8C peptide stimulation in CON8 neuronal cultures are shown as red boxes and downregulated DEGs in AD2-4 neuronal cultures are shown as green boxes. (**B**) Relative gene expression of *CALR, DYNC1H, LAMP2, HLA-DOA* and *HLA-DQB1* analyzed by RT-PCR. Data are presented as mean ± SEM from two independent experiments.

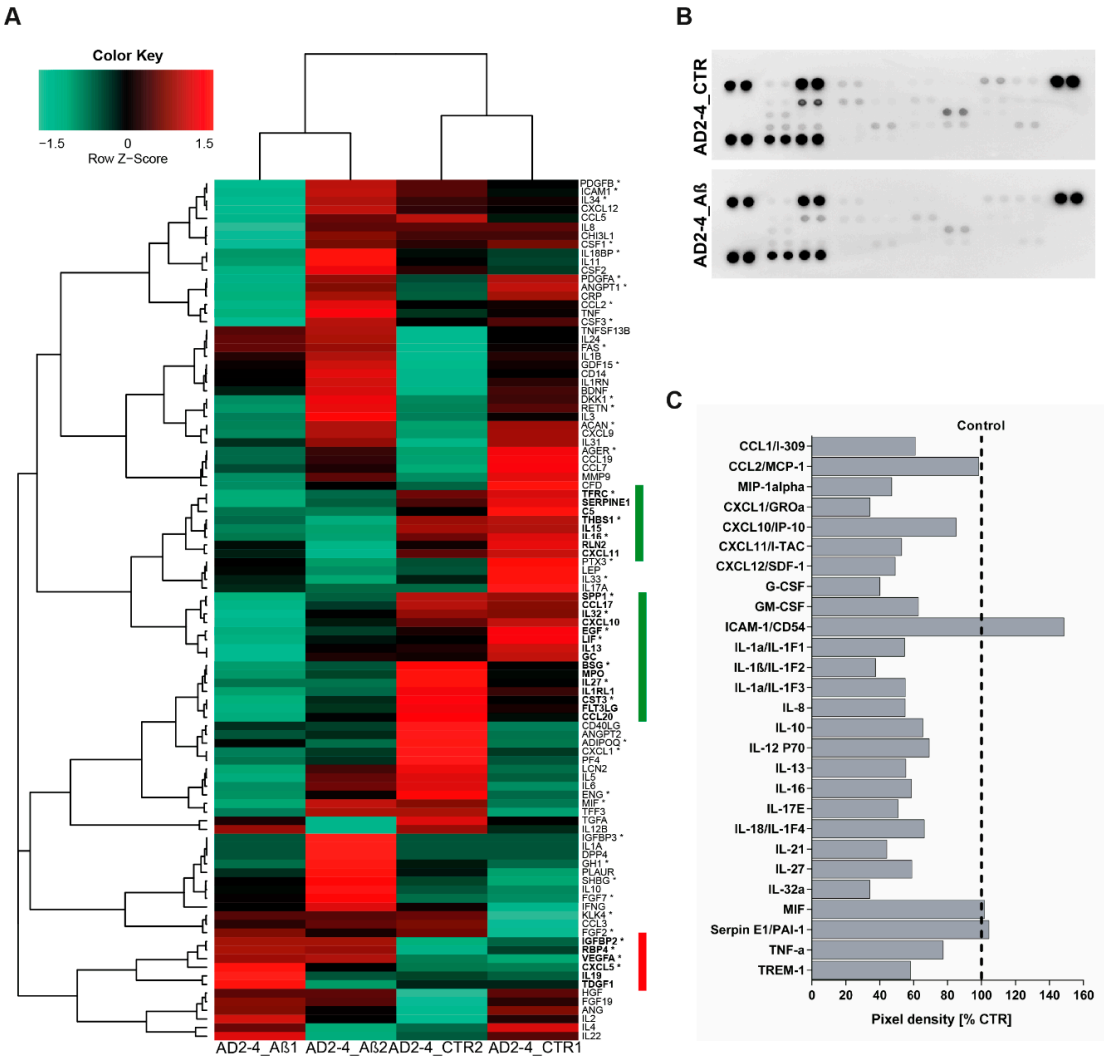

Figure 6. Analysis of cytokine expression and secreted factors in AD neuronal cultures upon Aβ-S8C stimulation. (**A**) Heatmap of Pearson correlation analysis of microarrays data from AD neural differentiation under Aβ-S8C stimulation (AD2-4_ Aβ1 and AD2-4_ Aβ2) or control (AD2-4_ CTR1 and AD2-4_ CTR2) showing the differential expression of cytokines. The highlighted genes in green represent a cluster of cytokines downregulated upon Aβ-S8C stimulation whereas the highlighted genes in red represent an upregulated cluster of cytokines. (**B**) Human cytokine array showing the effect of the Aβ-S8C peptide on the secreted factors of neuronal cultures from pooled AD2-2 and AD2-4 culture supernatants of control condition and 72 h of Aβ-S8C stimulation. (**C**) Quantitative analysis of the secreted factors shows that Aβ-S8C treatment decreases the amount of secreted cytokines in AD neuronal cultures.

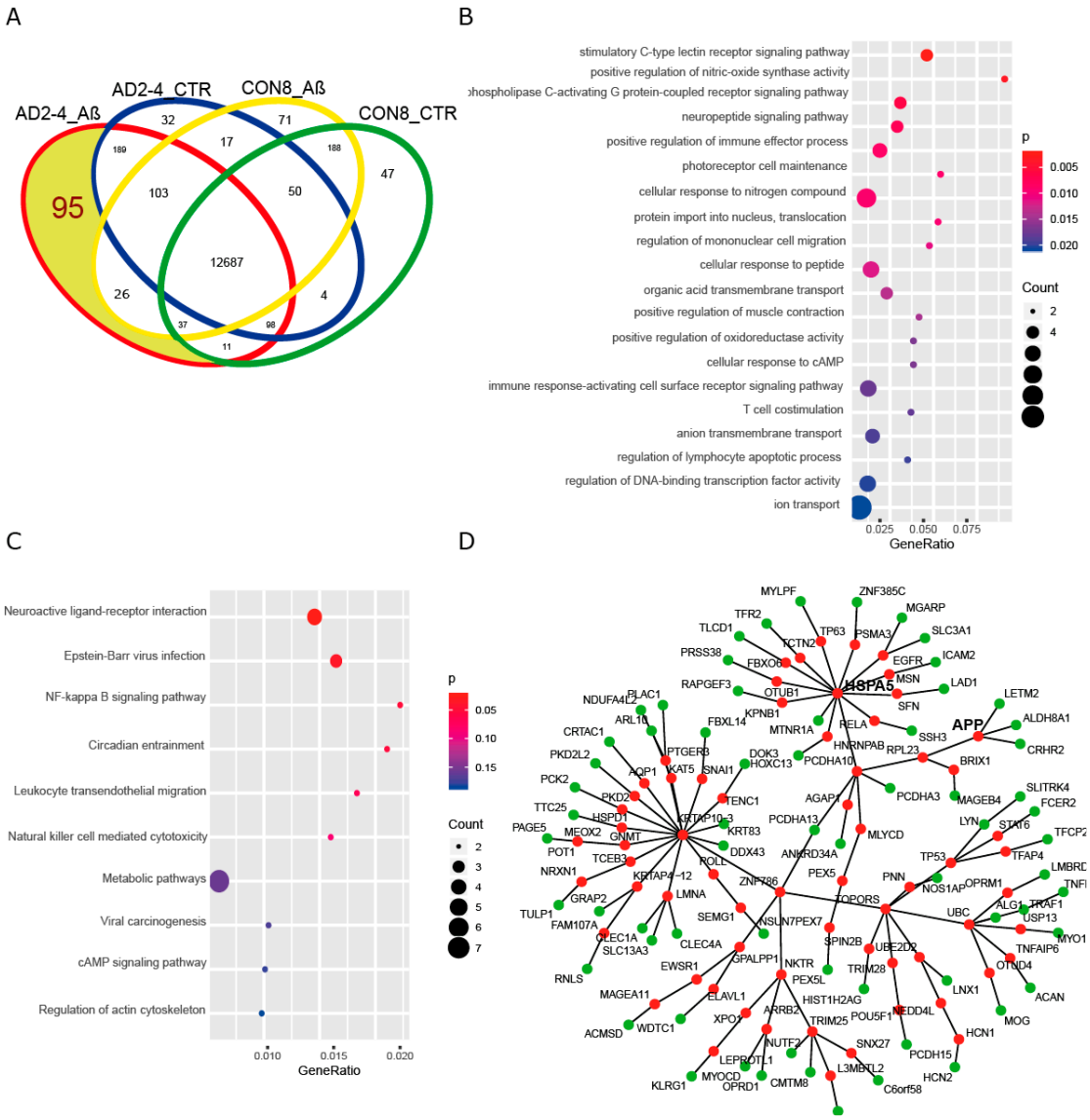

Figure 7. Aβ-S8C stimulated AD neuronal cultures activate a protein-protein interaction network, which includes APP and HSPA5. (**A**) Venn diagram dissecting 95 genes expressed in Aβ-S8C stimulated AD neuronal cultures from genes expressed in AD control and healthy neuronal cultures with and without Aβ-S8C stimulation. (**B**) Dot plot of gene ontologies (biological process) overrepresented in the 95 AD_Aβ genes. (**C**) Dot plot of KEGG pathways overrepresented in the 95 AD_Aβ genes. (**D**) Protein–protein interaction network derived from the 95 AD_Aβ genes with APP and HSPA5. Nodes from the 95 genes are colored green and the nodes added using the Biogrid database to connect the network are colored red.

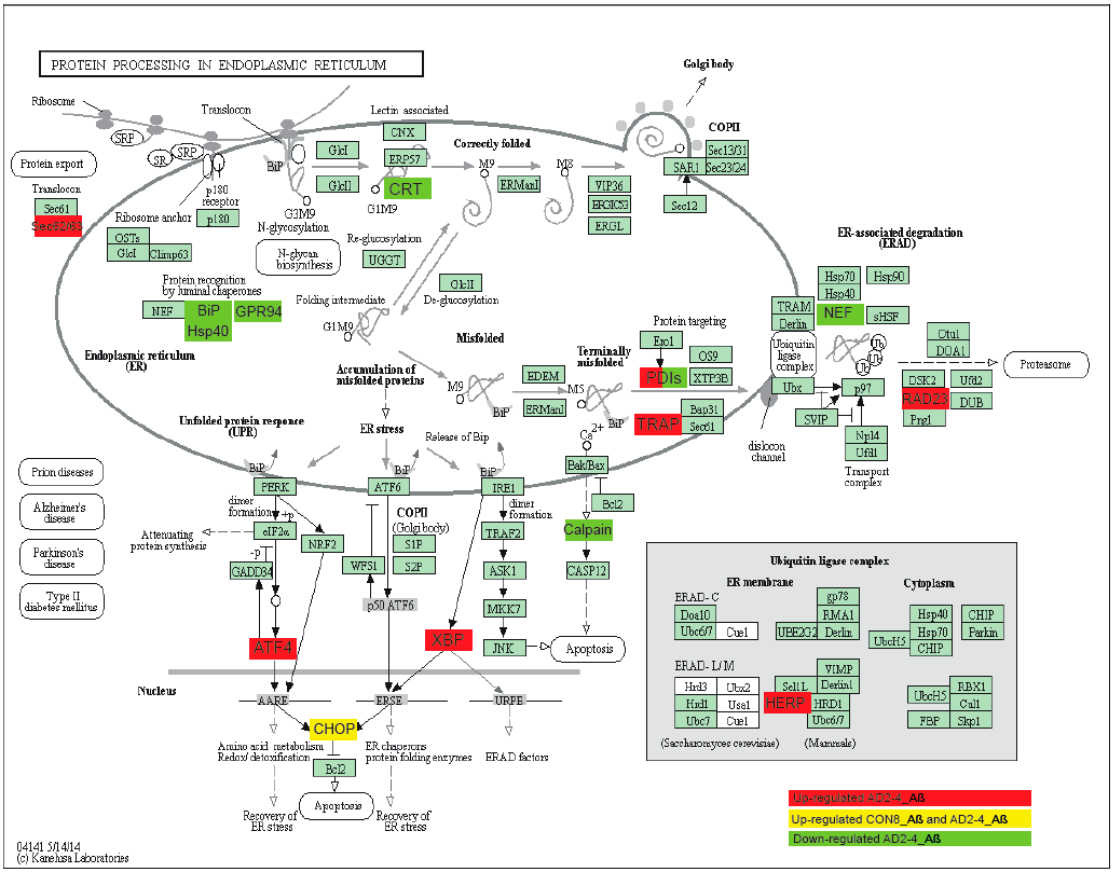

Figure 8. Representation of the KEGG protein process in endoplasmic reticulum pathway. Upregulated DEGs genes in response to Aβ-S8C stimulation in AD2-4 neuronal cultures are shown as red boxes, upregulated DEGs genes in response to Aβ-S8C stimulation in CON 8 and AD2-4 neuronal cultures are shown in yellow boxes and downregulated DEGs in AD2-4 neuronal cultures are shown as green boxes.

3. Discussion

While the mechanisms underlying the etiology of AD have been a focus of study over several decades, the current knowledge about the etiology and pathogenesis of AD are still incomplete. The use of primary neurons from animal models and immortalized cell lines based on modifications in *APP*, *PSEN1* and *PSEN2* has provided some insights into EOAD. While these models are helpful for studying a specific causal mutation (EOAD), there are several hurdles and limitations associated with studying LOAD, which requires the endogenous expression of genetic mutations and their genetic interactions. Understanding the biological implications of the recently identified genetic risk variants, namely the R47H substitution in *TREM2*, is essential to enable the establishment of genotype–phenotype correlations, which can lead to potential novel therapeutic approaches. The breakthrough development of iPSCs technology provides the most applicable tool to create an in vitro sporadic patient-derived model. Although modeling AD using patient-derived iPSCs has been prominent, a handful of studies to date have generated and characterized iPSC-derived neuronal cultures from LOAD patients [32,33,35,37,38]. This is the first study describing the generation and characterization of a model of LOAD based on Aβ dimer stimulated neuronal cultures originating from lymphoblast-derived iPSCs derived from LOAD patients carrying the missense mutation R47H in *TREM2*.

First, we differentiated the iPSCs to neurons using a modified protocol described by Liu et al., 2013 and analyzed the distinct progression steps during the differentiation process. Transcriptome analysis and immunocytochemistry confirmed the ability of our modified protocol to derive neurons and glia cells within our neuronal cultures. Based on gene expression comparison between the iPSC-neuronal

cultures with commercially bought fetal, adult and AD brain RNA we could show that our cells expressed the expected maturation markers. Thus, our results imply that lymphoblast-derived iPSCs from LOAD patients and healthy donors can be robustly differentiated into neuronal cultures. Moreover, we did not observe profound differences in the differentiation and maturation propensity between iPSCs derived from LOAD patients and healthy donors, in agreement with previous reports [33,35,37,38]. Cheng-Hathaway et al. and Sudom et al. reported that *Trem2* R47H knock-in mice showed reduced *Trem2* mRNA and protein expression in the brain as well as reduced soluble fragments of Trem2 (sTrem2) in plasma [66,67]. More recently, Xiang et al. reported that a mouse-specific splicing caused this reduction and *TREM2* mRNA levels were normal in both iPSC-derived microglia and in patient brains with the *TREM2* R47H variant [68]. We therefore evaluated if T*REM2* expression was different in LOAD patients carrying the *TREM2* R47H variant compared to the control. Our results indicate that *TREM2* mRNA was significantly upregulated in AD2-2 but not in the AD2-4 neuronal cultures compared to the control. This ambiguity is probably due to the limitations imposed by our small sample size. In addition, our neuronal culture is composed mainly of neurons so the TREM2 positive cells are in low abundance.

Although the neuronal cultures derived from LOAD patients and healthy donors did not exhibit differences in morphology or expression of differentiation markers, transcriptome analysis showed a distinct profile. Interestingly, GO analysis revealed that the proteins encoded by the 4990 genes exclusively expressed in AD neuronal cultures were predominantly mapped in the cell membrane and in the extracellular space. These genes were involved in (i) biological processes (BP) terms such as response to stimulus and secretion and (ii) molecular functions (MF) terms such as signal transducer activity, receptor activity, transporter activity, channel activity and ion transmembrane transporter activity. As part of these exclusively expressed genes we also identified genes of the matrix metalloproteinases (MMPs) family, for example *MMP2* and *MMP9*. Metalloproteinases play an important role in the pathogenesis of AD. While MMP2 might have a protective role, MMP9 expression, which is increased in AD patients, is induced by Aβ and it can influence TAU aggregation [69]. Furthermore, members of the ATP-binding cassette (ABC) and the solute carrier (SLC) families were over-represented in the GO_MF. ABC transporters have been implicated in AD pathophysiology, associated with processes leading to the accumulation of Aβ in the CNS. Importantly, we observed the exclusively expression of GLUT4 (*SLC2A4)*, a crucial insulin sensitive glucose transporter upregulated in AD patients, which is responsible for regulating glucose metabolism in neurons [70,71]. As anticipated, we also identified GO terms related to the regulation of the innate and adaptive immune response as significantly enriched. Implications of these results are that our AD neuronal cultures show a distinct signal transducer and transporter activity that may contribute to metabolic alterations, to an inadequate immune response and ultimately to neurotoxicity. According to the amyloid cascade theory, accumulation of Aβ plays a key role in triggering the cascade of events underlying the pathogenesis of EOAD. However some studies have shown that Aβ secretion is not altered in LOAD-derived neurons [37,72]. In accordance, our results show that AD cultures secreted Aβ with a similar $A\beta_{1\text{-}42}$ to $A\beta_{1\text{-}40}$ ratio as the control. Nonetheless, the levels of $A\beta_{1\text{-}40}$ and $A\beta_{1\text{-}42}$ were highly reproducible across multiple differentiations (six) and lines (four), thus establishing our cell culture model as robust for manipulating the production of Aβ. We subsequently aimed at evaluating the potential effect of Aβ in our neuronal cultures in order to close the gap in our understanding of the mechanisms that are underlying the early stages of AD. Aβ-S8C dimer can induce neurotoxicity and abnormal synaptic signaling, together with impaired cognitive functions in the absence of plaque pathology, thus mimicking the early stages of AD [55]. Aβ-induced TAU hyper-phosphorylation has been described to initiate the signaling cascade alterations that culminate in NFT formation and neuronal degeneration [73]. Phosphorylation of the AT8 epitope (Ser202/Thr205) has been found to be elevated in sAD-derived neurons [37]. We were not able to detect an increase in phosphorylation of TAU at Ser202/Thr205 upon Aβ-S8C dimer treatment. In addition, there were no differences in the levels of phosphorylation detected between control and AD neuronal cultures in the non-stimulated conditions. TAU can be phosphorylated on more than 80 residues,

and it is known that Ser422 is phosphorylated earlier than Ser202/Thr205 during NFTs formation [74]. Based on these facts and the results obtained, we can assume that the duration of incubation of the Aβ-S8C dimer was presumably not long enough to detect increased phosphorylation at Ser202/Thr205. Our results show that independent of the genetic background, incubation with the Aβ-S8C dimer increased the levels of total APP. A more in-depth analysis of APP processing will provide more insights into the pathogenic role of the *TREM2* R47H variant in EOAD.

In addition to interfering with total APP levels, Aβ-S8C dimer stimulation induced a remarkable and significant transcriptome change in the control as well as in the AD neuronal cultures. Annotation and enrichment analysis revealed that the upregulated DEGs induced by Aβ-S8C stimulation in the control neuronal cultures are related to immune system activation (interferon-gamma-mediated signaling pathway, cellular response to cytokine stimulus and adaptive immune response). Aβ soluble species have also been linked to an attenuation of the Wnt signaling pathway, in addition to putative effects on cell cycle, contributing to synaptic dysfunction and neurodegeneration. In accord, our data revealed that Wnt signaling and cell cycle were downregulated after Aβ-S8C stimulation in the control neuronal cultures. On the contrary, the AD neuronal cultures responded in a completely different manner to stimulation with the Aβ-S8C dimer.

The effect of the AD-associated TREM2 mutations on phagocytosis is an active area of study but so far variable results have been obtained. While R47H transduced HEK cells displayed a reduced up-take of latex beads and $A\beta_{1\text{-}42}$, no changes were observed in the fluorescent pH-sensitive rhodamine *Escherichia coli* (pHrodo-linked *E. coli)* uptake assay [61]. Additionally, *TREM2*$^{+/R47H}$ transdifferentiated microglia-like cells [58] and microglia-like cells derived from *TREM2* T66M $^{+/-}$, T66M $^{-/-}$ and W50C$^{-/-}$ hPSCs, also showed no defects in the *E. coli* uptake [59,63]. However, Piers et al. showed that iPSC-derived microglia harboring the *TREM2* R47H mutation exhibit a substantial deficil in the ability to phagocytose β-Amyloid [75]. We found that the control neuronal cultures upregulated the phagosome pathway after Aβ-S8C stimulation, namely the genes associated with MHCII. These observations are in line with previous reports where incubation with Aβ led to an accumulation of MHC-II and AD patients also showed upregulation of MHC-II [76]. On the contrary, these genes were not differentially regulated in our AD neuronal cultures, but interestingly other genes associated with the phagosome pathway were downregulated. Calreticulin is encoded by the *CALR* gene. It is an endoplasmic reticulum protein that interacts with Aβ, and is considered as a scavenger for $A\beta_{1\text{-}42}$ [77]. Low levels of calreticulin have been observed in AD brains, and it has been suggested that this down-regulation can lead to the pathological processes of AD [78]. Notably, the levels of tubulins *TUBB4A* and *TUBB4B* were downregulated, supported by Hondius et al., where the levels of these tubulins identified by mass spectrometry analysis in human post-mortem brain tissue were significantly decreased over the progressive stages of AD [79]. On the other hand, lysosome-associated membrane protein 2 (LAMP-2) together with other lysosome-related proteins was found to be increased in CSF from AD patients [80]. Interestingly, *LAMP2* was downregulated in our AD neuronal cultures leading us to speculate that R47H AD carriers have a unique response to phagocytosis, probably due to the partial loss of function of TREM2 activity.

The analysis of pro-inflammatory cytokines at the levels of mRNA and the secretome of the AD neuronal cultures in response to Aβ-S8C stimulation are of particular interest. Although the mRNA expression of the *IL-1β*, *IL-6*, *TNF-α* and *MIP-1α* proinflammatory cytokines was upregulated in some of the samples, the secretion of these cytokines was downregulated. A recent study using iPSC-derived microglia-like cells from patients carrying the T66M and W50C missense mutation within *TREM2* showed that these cells have a deficit in the cytokine release [63]. Indeed, *SPP1* and *GPNMB*, encoding osteopontin and osteoactivin, were also downregulated in AD neuronal cultures and not in the control after Aβ-S8C stimulation. SPP1 and GPNMB are microglia activation-related transcripts that are upregulated in AD models and associated with Aβ accumulation. In support of our data, it was recently reported that SPP1 and GPNMB reflect TREM2 signaling and the expression is highly sensitive to the R47H variant [26]. Interestingly, there was a cluster of genes associated with insulin

resistance, which was upregulated after Aβ-S8C stimulation. Increased levels of RBP4 were found in APP/PSEN1 mice and in insulin resistant humans [81]. Along the same track, it has been suggested that IGFBP2 plays a role in AD progression [82]. Both of these genes were indeed upregulated in response to Aβ-S8C in our AD neuronal cultures, thus further lending credence to the fact that metabolic dysfunction plays an important role in the pathogenesis of AD. It is noticeable that Aβ-S8C triggers a unique response in AD neuronal cultures, when compared to the control. The creation of a PPI network between the exclusively expressed genes in the AD after Aβ-S8C stimulation revealed *HSPA5* as the core of the Aβ-S8C signature. HSPA5, a chaperone protein that upon accumulation of unfolded proteins controls the activation of the UPR sensors [65], was found down-regulated after Aβ-S8C in our AD TREM2 neuronal cultures. Katayama et al. found that HSPA5 levels are reduced in the brains of AD patients [83]. Although Aβ-S8C stimulation upregulates *ATF3* and *DDIT3* (CHOP) in both CON and AD neuronal cultures, the prominent alteration in the UPR was observed in the AD TREM2 cultures with the upregulation of *XBP1, ATF4, BBC3, HERPUD1* and *CALR*. In support of our data, several studies have shown upregulation of the UPR in brain samples of AD patients [84,85]. According to Han et al. insufficient protein-folding homeostasis by URP increases expression of ATF4 and CHOP and initiates the ER-stress-mediated cell death, activating target genes involved in protein synthesis like aminoacyl-tRNA synthetases and RNA metabolic processes leading to oxidative stress and cell death [86]. Interestingly, biological processes related with increased protein synthesis such as amino acid activation and RNA metabolic process together with the KEGG pathway protein processing in the endoplasmic reticulum were upregulated in AD neuronal cultures. It seems that Aβ-S8C stimulation leads to the activation of the UPR that initially might be protective, however if the balance in proteostasis is not re-established, ER-stress-mediated cell death might mediate neurodegeneration in AD.

4. Materials and Methods

4.1. iPSC Lines

The iPSC lines derived from AD patients as well as control individuals without dementia used in this study have been characterized and published [40–43], as detailed in Table 1. All participants and/or their legal guardian provided written informed consent for participation in the study. Ethical approval was obtained by the Ethics Committee of the University Hospital Antwerp and the University of Antwerp (Approval number 13/15/161 obtained on 22 April 2013). AD patients were ascertained at the memory clinic of the ZNA Middelheim, Antwerpen, Belgium in the frame of a prospective study of neurodegenerative and vascular dementia in Flanders, Belgium. Ethnicity-matched healthy individuals were screened for neurological or psychiatric antecedents, neurological complaints and organic disease involving the central nervous system. Ascertainment and *TREM2* p.R47H genotyping are described in detail in [24]. iPSCs were maintained on Matrigel-coated (Corning, Bedford, MA, USA) plates in StemMACs culture medium (Miltenyi Biotec, Bergisch Gladbach, Germany). The medium was changed every day and the cells were passaged every 5–6 days using PBS without calcium and magnesium (Gibco, Life Technologies, Karlsruhe, Germany).

4.2. Neural Differentiation of the IPSC Lines

For the induction of GABAergic interneurons, iPSCs were differentiated using an embryoid body-based protocol [47] with modifications. On day 1, the iPS cells were harvested and recultivated in suspension in neural induction medium (NIM; DMEM/F-12 (Gibco, Life Technologies, Karlsruhe, Germany), 1% NEAA (Lonza, Basel, Switzerland), 1% N2 supplement (Gibco, Life Technologies, Karlsruhe, Germany), 2 µg/mL of Heparin (Sigma-Aldrich, Steinheim, Germany) and 1% P/S) supplemented with 1 µM purmorphamine (Tocris, Bristol, UK), a SHH agonist. At day 5 the formed aggregates, called embryoid bodies (EBs), were harvested and replated as adherent cells in the same medium and the same concentration of purmorphamine. From day 10 to 18, primitive

neuroepithelia structures were formed and neural rosettes were selected with STEMDiff Neural Rosette Selection reagent (Stem Cell Technologies, Vancouver, Canada) and recultured in suspension in NIM plus a B27 supplement (Gibco, Life Technologies, Karlsruhe, Germany; without retinoic acid) and 20 ng/mL of EGF and FGF2 (both PrepoTech, Hamburg, Germany). After 10 days the cells maintained as aggregates (neurospheres) were dissociated into single cells with accutase (Gibco, Life Technologies, Karlsruhe, Germany) and replated on Matrigel (Corning, Bedford, MA, USA) for the final differentiation in neural differentiating medium (NDM; Neurobasal 1% NEAA, 1% N2 supplement and 1% P/S) supplemented with 1µM of cAMP (Thermo Fisher Scientific, Rockford, IL, USA) and 10 ng/mL of BDNF, GDNF and IGF-1 (all Immuno Tools, Friesoythe, Germany). The iPSC-derived neurons were cultivated for approximately 80 days.

4.3. Cryosection of Neurospheres

Neurospheres were fixed in 4% paraformaldehyde (PFA) for 30 min at room temperature, washed with PBS and cryoprotected in 30% sucrose in PBS overnight at 4 °C. Subsequently, these neurospheres were transferred into embedding medium (Tissue-Tek OCT Compound 4583, Sakura Finetek), snap-frozen on dry ice and stored at −80 °C. Neurospheres were cut into 10 µm thin slides using a Leica CM3050 S cryostat (Leica Biosystems, Wetzlar, Germany).

4.4. Immunofluorescence Stainings

Cells were fixed with 4% paraformaldehyde for 15 min at room temperature (RT). Neurosphere slides were thawed, dried and rehydrated in PBS. Fixed cells and neurosphere slides were permeabilized with 0.2% Triton X-100 for 10 min and blocked with 3% BSA in PBS for 1 h. Samples were then incubated with the following primary antibodies overnight at 4 °C: mouse anti-PAX6 (1:1000, SySy, Goettingen, Germany # 153011), rabbit anti-Nestin (1:400, Sigma Aldrich, Steinheim, Germany #N5413), mouse anti-NKX2.1 (1:1000, Merck Millipore, Burlington, MA, USA #MAB5460), goat anti-SOX1 (1:200, R&D, Bristol, UK # MAB3369), mouse anti-FOXG1 (1:1000, Biozol, Eching, Germany # LS-C197226), mouse anti-βIII-tubulin (1:200, Cell Signaling, Danvers, MA, USA #TU-20), rabbit anti-MAP2 (1:1000, SySy, Goettingen, Germany #188002), guinea pig anti-GFAP (1:500, SySy, Goettingen, Germany #173004), guinea pig anti-Synapsin 1 (1:500, SySy, Goettingen, Germany #106004), mouse anti-SMI-3 (1:2000, Biolegend, San Diego, CA, USA #SMI-312R) and rabbit anti-GABA (1:1000, Sigma Aldrich, Steinheim, Germany #A2052). After washing with PBS, cells were then incubated with the appropriate secondary antibody conjugated with Alexa-488, Alexa-555 or Alexa-647 (1:500, Invitrogen, Thermo Fisher Scientific, Rockford, IL, USA) for 1 h at RT. The nuclear stain Hoechst 33258 (2 ug/mL, Sigma-Aldrich, Steinheim, Germany) was added at the time of the secondary antibody incubation. Slices were mounted in ImmuMount (Thermo Fisher Scientific, Rockford, IL, USA) and fluorescent images were obtained by a LSM 700 microscope (Carl Zeiss AG, Jena, Germany), and analyzed in Adobe Photoshop software CS6 (Adobe, USA).

4.5. Immunoblotting of Lysates from Aß-S8C Dimer Stimulated Cells

iPSC-derived neurons were differentiated for six weeks and then stimulated with 500 nM of oxidized S8C dimers [55] for 72 h. Cells were then washed three times with PBS and then lysed in PBS/1% NP40 + complete protease inhibitor cocktail (Sigma-Aldrich, Steinheim, Germany) and phosphatase inhibitor cocktail 2 (Sigma-Aldrich, Steinheim, Germany). Lysates were cleared by centrifugation at 20.000*g* for 10 min and quantified with the DC Protein assay Kit (Bio-Rad, Hercules, CA, USA). Of the lysates 25 µg were then separated on NuPAGE 4-12% Bis-Tris gels (Invitrogen, Thermo Fisher Scientific, Rockford, IL, USA) and blotted to a 0.2 µm nitrocellulose membrane for 2 h at 400 mA. The blots were blocked in PBS containing 5% skim milk and then probed with the following primary antibodies over night at 4 °C: mouse anti-total TAU (HT7, 1:1000, Thermo Fisher Scientific, Rockford, IL, USA#MN1000), mouse anti-phospho TAU Ser202/Thr205 (AT8, 1:1000, Thermo Fisher Scientific, Rockford, IL, USA#MN1020), rabbit anti-APP (CT15, 1:3500), rabbit anti-βactin (1:5000,

Sigma-Aldrich, Steinheim, Germany #A2066) and mouse anti βIII-tubulin (1:1000, Cell Signaling, Danvers, MA, USA #TU-20). After washing the blots three times with PBS/0.05%Tween20 they were incubated with the appropriate secondary antibody: goat anti-mouse IRDye 680RD and 800CW as well as goat anti-rabbit IRDye 680RD and 800CW (all from LI-COR Biosciences, Lincoln, NE, USA). Following three times washing with PBS/0.05% Tween20 the fluorescent signals were quantified by applying the Odyssey infrared imaging system (LI-COR Biosciences, Lincoln, NE, USA).

4.6. Measurement of Aß1-40 and Aß1-42 by ELISA

Aß1-40 and Aß1-42 concentrations from cleared supernatants of differentiated iPSCs were quantified by using the Amyloid beta 40/42 Human ELISA Kits (#KHB3441 and KHB3481; Thermo Fisher Scientific, Rockford, IL, USA) according to the manufacturer's recommendations. Results were normalized to the protein concentration of the cells. The cells were washed three times with PBS and lysed in PBS/ 1% NP40. The protein content was then measured with the DC Protein assay Kit (Bio-Rad, Hercules, CA, USA).

4.7. RNA Isolation and Quantitative RT-PCR

Total RNA was extracted from cell lysates using Direct-zol RNA Mini Prep kit (Zymo Research, Freiburg, Germany) in combination with peqGOLD TriFast (PeqLab Biotechnologie, Darmstadt, Germany) according to the manufacturer´s protocol. Of purified RNA 0.5 µg was used for first-strand cDNA synthesis using TaqMan reverse transcription reagent (Applied Biosystems, Rockford, IL, USA). cDNA was used for subsequent PCR. Real-time quantification of genes was conducted for three independent cultures from each iPSC-derived interneuron line using the SYBR®Green RT-PCR assay (Applied Biosystems, Waltham, Massachusetts, USA). Primer sequences are provided in Table S6 (Primers were purchased from Eurofins Genomics). Amplification, detection of specific gene products and quantitative analysis were performed using a 'ViiA7' sequence detection system (Applied Biosystem, Waltham, Massachusetts, USA). The expression levels were normalized relative to the expression of the housekeeping gene RPS16 using the comparative Ct-method $2^{-\Delta\Delta Ct}$.

4.8. Generation of Deep Sequencing Data

Deep sequencing data of cDNA from iPSC-derived neuronal cultures were generated at the Neuromics Support Facility at the VIB- University Antwerpen Center for Molecular Neurology. Sequence libraries were constructed using QuantSeq 3′ mRNA-Seq Library Prep Kit (Lexogen, Greenland, NH, USA). Sequencing was performed by Illumina NextSeq sequencing. Reads were single-end with a read length of 151. Samples from two independent experiments (n = 4 cell lines) were multiplexed onto the sequencing flow cell and the measured reads were demultiplexed for follow-up processing. Total RNA from human adult brain, human brain clinically diagnosed with AD and human fetal brain were purchased from BioChain®, Newark, CA USA

4.9. Analysis of Deep Sequencing Data

The demultiplexed fastq files were aligned against the GRCh38 genome with the HISAT2 (version 2.1.0) alignment software [87] using options for clipping the 50 bases at the 3′ end of each read. The exact HISAT2 command, which was mainly derived from the parameter optimizations of Barruzzo et al. [88], was:

hisat2 -p 7 –trim3 50 -N 1 -L 20 -i S,1,0.5 -D 25 -R 5 –mp 1,0 –sp 3,0 -x hisatindex/grch38 -U input.fastq.gz -S output.sam

The resulting BAM files were sorted by coordinates applying SAMtools software [89]. Reads were summarized per gene with the subread (1.6.1) featurecounts software [90] against the gencode.v22.annotation.gtf using parameter –t exon –g gene_id. Summarized reads were normalized in R using the voom normalization [91] algorithm from the limma package [92] filtering genes, which were expressed with CPM (counts per million) > 2 in at least two samples.

4.10. Analysis of Microarray Data

cDNA from iPSC-derived GABAergic interneurons from CON8 and AD-TREM2-4 untreated (CTR) and treated with Aß-S8C dimer was subjected to hybridization in duplicates on the GeneChip PrimeView Human Gene Expression Array (Affymetrix, Thermo Fisher Scientific, Rockford, IL, USA) at the BMFZ (Biomedizinisches Forschungszentrum) core facility of the Heinrich-Heine University, Düsseldorf. Data analysis of the Affymetrix raw data was performed in the R/Bioconductor [93] environment using the package affy [94]. The obtained data were background-corrected and normalized by employing the robust multi-array average (RMA) method from the package affy. Hierarchical clustering dendrograms and heatmaps were generated using the heatmap.2 function from the gplots package with Pearson correlation as similarity measure and color scaling per genes [95]. Expressed genes were compared in Venn diagrams employing package VennDiagram [96]. Gene expression was assessed with a threshold of 0.05 for the detection-*p*-value, which was calculated as described in the supplementary methods in Graffmann et al. [97]. The datasets generated and analyzed during the current study are available in the GEO repository (https://www.ncbi.nlm.nih.gov/geo/) under the accession number GSE143951.

4.11. Protein Interaction Network

A protein interaction network was constructed from the set of 95 genes expressed exclusively in Aβ-S8C stimulated TREM2 neurons in the Venn diagram analysis. Interactions associated with *Homo sapiens* (taxonomy id 9606) were filtered from the Biogrid database version 3.4.161 [98]. From this dataset interactors and additionally interactors of these interactors starting at the proteins coded by the above-mentioned set of 95 genes were extracted. The resulting complex network was reduced by searching the shortest paths between the original set via the method get.shortest.paths () from the R package igraph [99]. The protein network consisting of these shortest paths was plotted employing the R package network [100] marking proteins from the original set in green and inferred proteins in red.

4.12. Gene Ontology and Pathway Analysis

Based on the set of 95 genes expressed exclusively in Aβ-S8C stimulated TREM2 neurons in the Venn diagram analysis over-represented gene ontology terms and KEGG (Kyoto Encyclopedia of Genes and Genomes) pathways [101] were determined. The hypergeometric test was used for over-representation analysis—in the version from the GOstats package [102] for GO terms and the version from the R base package for KEGG pathways, which had been downloaded from the KEGG database in March 2018. Dot plots of the most significant GO terms and KEGG pathways were done via the function ggplot() from the R package ggplot2 indicating *p*-values from the hypergeometric test on a red-blue color scale, number of significant genes in the dedicated pathway (G) by the size of the dots and ratios of the number of significant genes in the dedicated pathway/GO to the total number of genes in that pathway/GO on the x-axis.

4.13. Human Cytokine Array

The secretion of cytokines in AD neuronal cultures before and after stimulation with the Aß-S8C dimer was measured employing the Proteome Profiler Human Cytokine Array kit (R&D System, USA). The assay was performed following the manufacturer's instructions. Briefly, AD2-2 and AD2-4 cell culture supernatants from control and 72 h of Aß-S8C dimer stimulation were collected, pooled and mixed with a cocktail of biotinylated detection antibodies for further incubation in a nitrocellulose cytokine array membrane with the immobilized capture antibodies spotted in duplicates. Chemiluminescent detection of the streptavidin-HRP secondary antibody was performed and the average signal (pixel density) was determined for the pair of duplicate spots using Image J (U.S. National Institutes of Health, Bethesda, Maryland, MD, USA). The relative change in cytokine levels

was performed comparing the intensity of the spots in the Aß-S8C dimer stimulated membrane with the control membrane, which was set to 100%.

4.14. Statistical Analysis

Statistical analysis was performed with GraphPad Prism Software version 6.01 (GraphPad software, San Diego, CA, USA). For comparisons of the mean between two groups, one-tail Student´s *t*-test was performed. One-way ANOVA was used for statistical significance analysis for comparisons of the mean among 4 groups, followed by a post hoc test with the use of Tukey´s multiple comparison test. Statistical significance was assumed at $p < 0.05$. All data are expressed as mean ± standard error of the mean (SEM).

5. Conclusions

Our established neuronal cultures using lymphoblast-derived iPSCs from patients harboring the R47H mutation in TREM2 is a relevant model for investigating the effect of this variant in the etiology of LOAD. Comparative global transcriptome analysis identified a distinct gene expression profile in AD neuronal cultures, further suggesting that these lines exhibit alteration in key signaling pathways related to metabolism and immune system in comparison to control, thus implying the partial loss of function of TREM2 due to the R47H substitution. In addition, stimulation with the Aβ-S8C dimer revealed metabolic dysregulation, impaired phagocytosis-related pathway and altered inflammatory responses. Furthermore, our data strongly suggests that the Aβ-S8C dimer signature seems to be centered in the ER-stress response. In conclusion, our AD in vitro model is capable of efficiently responding to signaling cascades associated with the AD pathogenesis and thus is a promising cellular tool for investigating the molecular mechanisms underlying LOAD. Additionally, this cellular model can facilitate the discovery of new AD biomarkers, enable toxicology studies as well as the identification of potential drug targets for future therapy of this devastating disease.

Supplementary Materials: Supplementary materials can be found at http://www.mdpi.com/1422-0067/21/12/4516/s1.

Author Contributions: Conceptualization: S.M. and J.A.; Methodology: S.M., A.M.-S., L.E., M.B.; Formal analysis: S.M., A.M.-S., W.W., J.A.; Data curation: W.W.; Investigation: S.M., A.M.-S., M.B.; Resources: K.S., C.V.B. and C.K.; Writing—original draft preparation: S.M.; Writing—review and editing: J.A., W.W., A.M.-S., K.S., C.V.B., C.K.; Supervision: J.A. All authors have read and agreed to the published version of the manuscript.

Funding: JA acknowledges support from the Medical Faculty, Heinrich-Heine-University, Düsseldorf. JA, KS and CVB are members of the EU project—AgedBrainSYSBIO. The AgedBrainSYSBIO project received funding from the European Union's Seventh Framework Program for research, technological development and demonstration under grant agreement no 305299. Research at the Antwerp site is supported in part by the University of Antwerp Research Fund.

Acknowledgments: We thank Friederike Schröter for helping with the neuronal differentiations. We also thank the Zentrum für Informations- und Medientechnologie (ZIM) at the Heinrich-Heine University for the computational support.

Conflicts of Interest: The authors declare no conflict of interest.

References

1. Patterson, C. World Alzheimer Report 2018 The state of the art of dementia research: New frontiers. *Alzheimer's Dis. Int.* **2018**. [CrossRef]
2. Prince, M.; Comas-Herrera, A. Dementia Fact Sheet. *WHO*. 2017. Available online: https://www.who.int/news-room/fact-sheets/detail/dementia (accessed on 27 May 2020).
3. Hardy, J.A.; Higgins, G.A. Alzheimer's disease: The amyloid cascade hypothesis. *Science* **1992**, *256*, 184–185. [CrossRef] [PubMed]
4. Polanco, J.C.; Li, C.; Bodea, L.G.; Martinez-Marmol, R.; Meunier, F.A.; Götz, J. Amyloid-β and tau complexity - Towards improved biomarkers and targeted therapies. *Nat. Rev. Neurol.* **2018**, *14*, 22–40. [CrossRef] [PubMed]

5. Hardy, J.; Selkoe, D.J. The amyloid hypothesis of Alzheimer's disease: Progress and problems on the road to therapeutics. *Science* **2002**, *297*, 353–356. [CrossRef]
6. Cacace, R.; Sleegers, K.; van Broeckhoven, C. Molecular genetics of early-onset Alzheimer's disease revisited. *Alzheimer's Dement.* **2016**, *12*, 733–748. [CrossRef]
7. Carmona, S.; Hardy, J.; Guerreiro, R. The genetic landscape of Alzheimer disease. *Handb. Clin. Neurol.* **2018**, *148*, 395–408.
8. Bettens, K.; Sleegers, K.; Van Broeckhoven, C. Genetic insights in Alzheimer's disease. *Lancet Neurol.* **2013**, *12*, 92–104. [CrossRef]
9. Farrer, L.A.; Cupples, L.A.; Haines, J.L.; Hyman, B.; Kukull, W.A.; Mayeux, R.; Myers, R.H.; Pericak-Vance, M.A.; Risch, N.; Duijn, C.M. van Effects of Age, Sex, and Ethnicity on the Association Between Apolipoprotein E Genotype and Alzheimer Disease. *JAMA* **1997**, *278*, 1349. [CrossRef]
10. Bickeböller, H.; Campion, D.; Brice, A.; Amouyel, P.; Hannequin, D.; Didierjean, O.; Penet, C.; Martin, C.; Pérez-Tur, J.; Michon, A.; et al. Apolipoprotein E and Alzheimer disease: Genotype-specific risks by age and sex. *Am. J. Hum. Genet.* **1997**, *60*, 439–446.
11. Harold, D.; Abraham, R.; Hollingworth, P.; Sims, R. Genome-wide association study identifies variants at CLU and PICALM associated with Alzheimer's disease. *Nat. Genet.* **2009**, *41*, 1008–1093.
12. Hollingworth, P.; Harold, D.; Sims, R.; Gerrish, A.; Lambert, J.C.; Carrasquillo, M.M.; Abraham, R.; Hamshere, M.L.; Pahwa, J.S.; Moskvina, V.; et al. Common variants at ABCA7, MS4A6A/MS4A4E, EPHA1, CD33 and CD2AP are associated with Alzheimer's disease. *Nat. Genet.* **2011**, *43*, 429–435. [CrossRef] [PubMed]
13. Lambert, J.C.; Heath, S.; Even, G.; Campion, D.; Sleegers, K.; Hiltunen, M.; Combarros, O.; Zelenika, D.; Bullido, M.J.; Tavernier, B.; et al. Genome-wide association study identifies variants at CLU and CR1 associated with Alzheimer's disease. *Nat. Genet.* **2009**, *41*, 1094–1099. [CrossRef] [PubMed]
14. Naj, A.C.; Jun, G.; Beecham, G.W.; Wamg, L.-S.; Vardarajan, B.N.; Buros, J.; Gallins, P.J.; Buxbaum, J.D.; Jarvik, G.P.; Crane, P.k.; et al. Common variants at MS4A4/MS4A6E, CD2AP, CD33 and EPHA1 are associated with late-onset Alzheimer's disease. *Nat. Genet.* **2011**, *43*, 436–441. [CrossRef]
15. Seshadri, S.; AL, F.; MA, I.; AL, D.; Gudnason, V.; Boada, M.; JC, B.; AV, S.; MM, C.; JC, L.; et al. Genome-wide analysis of genetic loci associated with Alzheimer disease. *JAMA J. Am. Med. Assoc.* **2010**, *303*, 1832–1840. [CrossRef] [PubMed]
16. Bellenguez, C.; Grenier-Boley, B.; Lambert, J.-C. Genetics of Alzheimer's disease: Where we are, and where we are going. *Curr. Opin. Neurobiol.* **2020**, *61*, 40–48. [CrossRef] [PubMed]
17. Verheijen, J.; Sleegers, K. Understanding Alzheimer Disease at the Interface between Genetics and Transcriptomics. *Trends Genet.* **2018**, *34*, 434–447. [CrossRef]
18. Van Cauwenberghe, C.; van Broeckhoven, C.; Sleegers, K. The genetic landscape of Alzheimer disease: Clinical implications and perspectives. *Genet. Med.* **2016**, *18*, 421–430. [CrossRef]
19. Guerreiro, R.; Wojtas, A.; Bras, J.; Carrasquillo, M.; Rogaeva, E.; Majounie, E.; Cruchaga, C.; Sassi, C.; Kauwe, J.S.K.; Younkin, S.; et al. TREM2 variants in Alzheimer's disease. *N. Engl. J. Med.* **2013**, *368*, 117–127. [CrossRef]
20. Jonsson, T.; Stefansson, H.; Steinberg, S.; Jonsdottir, I.; Jonsson, P.V.; Snaedal, J.; Bjornsson, S.; Huttenlocher, J.; Levey, A.I.; Lah, J.J.; et al. Variant of TREM2 associated with the risk of Alzheimer's disease. *N. Engl. J. Med.* **2013**, *368*, 107–116. [CrossRef]
21. Song, W.; Hooli, B.; Mullin, K.; Jin, S.C.; Cella, M.; Ulland, T.K.; Wang, Y.; Tanzi, R.E.; Colonna, M. Alzheimer's disease-associated TREM2 variants exhibit either decreased or increased ligand-dependent activation. *Alzheimer's Dement.* **2017**, *13*, 381–387. [CrossRef]
22. Sims, R.; van der Lee, S.J.; Naj, A.C.; Bellenguez, C.; Badarinarayan, N.; Jakobsdottir, J.; Kunkle, B.W.; Boland, A.; Raybould, R.; Bis, J.C.; et al. Rare coding variants in PLCG2, ABI3, and TREM2 implicate microglial-mediated innate immunity in Alzheimer's disease. *Nat. Genet.* **2017**, *49*, 1373–1384. [CrossRef] [PubMed]
23. Ruiz, A.; Dols-Icardo, O.; Bullido, M.J.; Pastor, P.; Rodríguez-Rodríguez, E.; López de Munain, A.; de Pancorbo, M.M.; Pérez-Tur, J.; Álvarez, V.; Antonell, A.; et al. Assessing the role of the TREM2 p.R47H variant as a risk factor for Alzheimer's disease and frontotemporal dementia. *Neurobiol. Aging* **2014**, *35*, 444.e1–444.e4. [CrossRef] [PubMed]

24. Cuyvers, E.; Bettens, K.; Philtjens, S.; Van Langenhove, T.; Gijselinck, I.; van der Zee, J.; Engelborghs, S.; Vandenbulcke, M.; Van Dongen, J.; Geerts, N.; et al. Investigating the role of rare heterozygous TREM2 variants in Alzheimer's disease and frontotemporal dementia. *Neurobiol. Aging* **2014**, *35*. [CrossRef] [PubMed]
25. Colonna, M.; Wang, Y. TREM2 variants: New keys to decipher Alzheimer disease pathogenesis. *Nat. Rev. Neurosci.* **2016**, *17*, 201–207. [CrossRef] [PubMed]
26. Song, W.M.; Joshita, S.; Zhou, Y.; Ulland, T.K.; Gilfillan, S.; Colonna, M. Humanized TREM2 mice reveal microglia-intrinsic and -extrinsic effects of R47H polymorphism. *J. Exp. Med.* **2018**, *215*, 745–760. [CrossRef]
27. Wang, Y.; Cella, M.; Mallinson, K.; Ulrich, J.D.; Young, K.L.; Robinette, M.L.; Gilfillan, S.; Krishnan, G.M.; Sudhakar, S.; Zinselmeyer, B.H.; et al. TREM2 lipid sensing sustains the microglial response in an Alzheimer's disease model. *Cell* **2015**, *160*, 1061–1072. [CrossRef]
28. Jay, T.R.; Miller, C.M.; Cheng, P.J.; Graham, L.C.; Bemiller, S.; Broihier, M.L.; Xu, G.; Margevicius, D.; Karlo, J.C.; Sousa, G.L.; et al. TREM2 deficiency eliminates TREM2+ inflammatory macrophages and ameliorates pathology in Alzheimer's disease mouse models. *J. Exp. Med.* **2015**, *212*, 287–295. [CrossRef]
29. Yuan, P.; Condello, C.; Keene, C.D.; Wang, Y.; Bird, T.D.; Paul, S.M.; Luo, W.; Colonna, M.; Baddeley, D.; Grutzendler, J. TREM2 Haplodeficiency in Mice and Humans Impairs the Microglia Barrier Function Leading to Decreased Amyloid Compaction and Severe Axonal Dystrophy. *Neuron* **2016**, *90*, 724–739. [CrossRef]
30. Lee, C.Y.D.; Daggett, A.; Gu, X.; Jiang, L.L.; Langfelder, P.; Li, X.; Wang, N.; Zhao, Y.; Park, C.S.; Cooper, Y.; et al. Elevated TREM2 Gene Dosage Reprograms Microglia Responsivity and Ameliorates Pathological Phenotypes in Alzheimer's Disease Models. *Neuron* **2018**, *97*, 1032–1048.e5. [CrossRef]
31. Zhao, Y.; Wu, X.; Li, X.; Jiang, L.-L.; Gui, X.; Liu, Y.; Sun, Y.; Zhu, B.; Piña-Crespo, J.C.; Zhang, M.; et al. TREM2 Is a Receptor for β-Amyloid that Mediates Microglial Function. *Neuron* **2018**, *97*, 1023–1031.e7. [CrossRef]
32. Muratore, C.R.; Rice, H.C.; Srikanth, P.; Callahan, D.G.; Shin, T.; Benjamin, L.N.P.; Walsh, D.M.; Selkoe, D.J.; Young-Pearse, T.L. The familial Alzheimer's disease APPV717I mutation alters APP processing and Tau expression in iPSC-derived neurons. *Hum. Mol. Genet.* **2014**, *23*, 3523–3536. [CrossRef] [PubMed]
33. Hossini, A.M.; Megges, M.; Prigione, A.; Lichtner, B.; Toliat, M.R.; Wruck, W.; Schröter, F.; Nuernberg, P.; Kroll, H.; Makrantonaki, E.; et al. Induced pluripotent stem cell-derived neuronal cells from a sporadic Alzheimer's disease donor as a model for investigating AD-associated gene regulatory networks. *BMC Genomics* **2015**, *16*, 84. [CrossRef]
34. Yagi, T.; Ito, D.; Okada, Y.; Akamatsu, W.; Nihei, Y.; Yoshizaki, T.; Yamanaka, S.; Okano, H.; Suzuki, N. Modeling familial Alzheimer's disease with induced pluripotent stem cells. *Hum. Mol. Genet.* **2011**, *20*, 4530–4539. [CrossRef] [PubMed]
35. Israel, M.A.; Yuan, S.H.; Bardy, C.; Reyna, S.M.; Mu, Y.; Herrera, C.; Hefferan, M.P.; Van Gorp, S.; Nazor, K.L.; Boscolo, F.S.; et al. Probing sporadic and familial Alzheimer's disease using induced pluripotent stem cells. *Nature* **2012**, *482*, 216–220. [CrossRef]
36. Duan, L.; Bhattacharyya, B.J.; Belmadani, A.; Pan, L.; Miller, R.J.; Kessler, J.A. Stem cell derived basal forebrain cholinergic neurons from Alzheimer's disease patients are more susceptible to cell death. *Mol. Neurodegener.* **2014**, *9*, 3. [CrossRef]
37. Ochalek, A.; Mihalik, B.; Avci, H.X.; Chandrasekaran, A.; Téglási, A.; Bock, I.; Lo Giudice, M.; Táncos, Z.; Molnár, K.; László, L.; et al. Neurons derived from sporadic Alzheimer's disease iPSCs reveal elevated TAU hyperphosphorylation, increased amyloid levels, and GSK3B activation. *Alzheimers. Res. Ther.* **2017**, *9*, 90. [CrossRef]
38. Flamier, A.; El Hajjar, J.; Adjaye, J.; Fernandes, K.J.; Abdouh, M.; Bernier, G. Modeling Late-Onset Sporadic Alzheimer's Disease through BMI1 Deficiency. *Cell Rep.* **2018**, *23*, 2653–2666. [CrossRef]
39. Zhang, B.; Gaiteri, C.; Bodea, L.-G.; Wang, Z.; McElwee, J.; Podtelezhnikov, A.A.; Zhang, C.; Xie, T.; Tran, L.; Dobrin, R.; et al. Integrated Systems Approach Identifies Genetic Nodes and Networks in Late-Onset Alzheimer's Disease. *Cell* **2013**, *153*, 707–720. [CrossRef]
40. Martins, S.; Bohndorf, M.; Schröter, F.; Assar, F.; Wruck, W.; Sleegers, K.; Van Broeckhoven, C.; Adjaye, J. Lymphoblast-derived integration-free ISRM-CON9 iPS cell line from a 75 year old female. *Stem Cell Res.* **2018**, *26*. [CrossRef]

41. Schröter, F.; Sleegers, K.; Cuyvers, E.; Bohndorf, M.; Wruck, W.; Van Broeckhoven, C.; Adjaye, J. Lymphoblast-derived integration-free iPS cell line from a female 67-year-old Alzheimer's disease patient with TREM2 (R47H) missense mutation. *Stem Cell Res.* **2016**, *17*, 553–555. [CrossRef]
42. Schröter, F.; Sleegers, K.; Cuyvers, E.; Bohndorf, M.; Wruck, W.; Van Broeckhoven, C.; Adjaye, J. Lymphoblast-derived integration-free iPS cell line from a 65-year-old Alzheimer's disease patient expressing the TREM2 p.R47H variant. *Stem Cell Res.* **2016**, *16*, 113–115. [CrossRef] [PubMed]
43. Schröter, F.; Sleegers, K.; Bohndorf, M.; Wruck, W.; Van Broeckhoven, C.; Adjaye, J. Lymphoblast-derived integration-free iPS cell line from a 69-year-old male. *Stem Cell Res.* **2016**, *16*, 29–31. [CrossRef] [PubMed]
44. Levenga, J.; Krishnamurthy, P.; Rajamohamedsait, H.; Wong, H.; Franke, T.F.; Cain, P.; Sigurdsson, E.M.; Hoeffer, C.A. Tau pathology induces loss of GABAergic interneurons leading to altered synaptic plasticity and behavioral impairments. *Acta Neuropathol. Commun.* **2013**, *1*, 34. [CrossRef] [PubMed]
45. Burgos-Ramos, E.; Hervás-Aguilar, A.; Aguado-Llera, D.; Puebla-Jiménez, L.; Hernández-Pinto, A.M.; Barrios, V.; Arilla-Ferreiro, E. Somatostatin and Alzheimer's disease. *Mol. Cell. Endocrinol.* **2008**, *286*, 104–111. [CrossRef] [PubMed]
46. Jo, S.; Yarishkin, O.; Hwang, Y.J.; Chun, Y.E.; Park, M.; Woo, D.H.; Bae, J.Y.; Kim, T.; Lee, J.; Chun, H.; et al. GABA from reactive astrocytes impairs memory in mouse models of Alzheimer's disease. *Nat. Med.* **2014**, *20*, 886–896. [CrossRef] [PubMed]
47. Liu, Y.; Liu, H.; Sauvey, C.; Yao, L.; Zarnowska, E.D.; Zhang, S.-C. Directed differentiation of forebrain GABA interneurons from human pluripotent stem cells. *Nat. Protoc.* **2013**, *8*, 1670–1679. [CrossRef]
48. Li, J.T.; Zhang, Y. TREM2 regulates innate immunity in Alzheimer's disease. *J. Neuroinflammation* **2018**, *15*, 107. [CrossRef]
49. Sengupta, U.; Nilson, A.N.; Kayed, R. The Role of Amyloid-β Oligomers in Toxicity, Propagation, and Immunotherapy. *EBioMedicine* **2016**, *6*, 42. [CrossRef]
50. Viola, K.L.; Klein, W.L. Amyloid β oligomers in Alzheimer's disease pathogenesis, treatment, and diagnosis. *Acta Neuropathol.* **2015**, *129*, 183–206. [CrossRef]
51. Klyubin, I.; Betts, V.; Welzel, A.T.; Blennow, K.; Zetterberg, H.; Wallin, A.; Lemere, C.A.; Cullen, W.K.; Peng, Y.; Wisniewski, T.; et al. Amyloid Protein Dimer-Containing Human CSF Disrupts Synaptic Plasticity: Prevention by Systemic Passive Immunization. *J. Neurosci.* **2008**, *28*, 4231–4237. [CrossRef]
52. Shankar, G.M.; Li, S.; Mehta, T.H.; Garcia-Munoz, A.; Shepardson, N.E.; Smith, I.; Brett, F.M.; Farrell, M.A.; Rowan, M.J.; Lemere, C.A.; et al. Amyloid-β protein dimers isolated directly from Alzheimer's brains impair synaptic plasticity and memory. *Nat. Med.* **2008**, *14*, 837–842. [CrossRef] [PubMed]
53. Mc Donald, J.M.; Savva, G.M.; Brayne, C.; Welzel, A.T.; Forster, G.; Shankar, G.M.; Selkoe, D.J.; Ince, P.G.; Walsh, D.M.; Medical Research Council. Cognitive Function and Ageing Study The presence of sodium dodecyl sulphate-stable Aβ dimers is strongly associated with Alzheimer-type dementia. *Brain* **2010**, *133*, 1328–1341. [CrossRef] [PubMed]
54. Brinkmalm, G.; Hong, W.; Wang, Z.; Liu, W.; O'Malley, T.T.; Sun, X.; Frosch, M.P.; Selkoe, D.J.; Portelius, E.; Zetterberg, H.; et al. Identification of neurotoxic cross-linked amyloid-β dimers in the Alzheimer's brain. *Brain* **2019**, *142*, 1441–1457. [CrossRef] [PubMed]
55. Müller-Schiffmann, A.; Herring, A.; Abdel-Hafiz, L.; Chepkova, A.N.; Schäble, S.; Wedel, D.; Horn, A.H.C.; Sticht, H.; de Souza Silva, M.A.; Gottmann, K.; et al. Amyloid-β dimers in the absence of plaque pathology impair learning and synaptic plasticity. *Brain* **2016**, *139*, 509–525. [CrossRef]
56. Abdel-Hafiz, L.; Müller-Schiffmann, A.; Korth, C.; Fazari, B.; Chao, O.Y.; Nikolaus, S.; Schäble, S.; Herring, A.; Keyvani, K.; Lamounier-Zepter, V.; et al. Aβ dimers induce behavioral and neurochemical deficits of relevance to early Alzheimer's disease. *Neurobiol. Aging* **2018**, *69*, 1–9. [CrossRef]
57. Müller-Schiffmann, A.; Andreyeva, A.; Horn, A.H.C.; Gottmann, K.; Korth, C.; Sticht, H. Molecular Engineering of a Secreted, Highly Homogeneous, and Neurotoxic Aβ Dimer. *ACS Chem. Neurosci.* **2011**, *2*, 242–248. [CrossRef]
58. Claes, C.; Van Den Daele, J.; Boon, R.; Schouteden, S.; Colombo, A.; Monasor, L.S.; Fiers, M.; Ordovás, L.; Nami, F.; Bohrmann, B.; et al. Human stem cell–derived monocytes and microglia-like cells reveal impaired amyloid plaque clearance upon heterozygous or homozygous loss of TREM2. *Alzheimer's Dement.* **2018**, *15*, 453–464. [CrossRef]

59. Brownjohn, P.W.; Smith, J.; Solanki, R.; Lohmann, E.; Houlden, H.; Hardy, J.; Dietmann, S.; Livesey, F.J. Functional Studies of Missense TREM2 Mutations in Human Stem Cell-Derived Microglia. *Stem Cell Rep.* **2018**, *10*, 1294–1307. [CrossRef]
60. Hsieh, C.L.; Koike, M.; Spusta, S.C.; Niemi, E.C.; Yenari, M.; Nakamura, M.C.; Seaman, W.E. A role for TREM2 ligands in the phagocytosis of apoptotic neuronal cells by microglia. *J. Neurochem.* **2009**, *109*, 1144–1156. [CrossRef]
61. Kleinberger, G.; Yamanishi, Y.; Suarez-Calvet, M.; Czirr, E.; Lohmann, E.; Cuyvers, E.; Struyfs, H.; Pettkus, N.; Wenninger-Weinzierl, A.; Mazaheri, F.; et al. TREM2 mutations implicated in neurodegeneration impair cell surface transport and phagocytosis. *Sci. Transl. Med.* **2014**, *6*, 243ra86. [CrossRef]
62. Takahashi, K.; Rochford, C.D.P.; Neumann, H. Clearance of apoptotic neurons without inflammation by microglial triggering receptor expressed on myeloid cells-2. *J. Exp. Med.* **2005**, *201*, 647–657. [CrossRef] [PubMed]
63. Garcia-Reitboeck, P.; Phillips, A.; Piers, T.M.; Villegas-Llerena, C.; Butler, M.; Mallach, A.; Rodrigues, C.; Arber, C.E.; Heslegrave, A.; Zetterberg, H.; et al. Human Induced Pluripotent Stem Cell-Derived Microglia-Like Cells Harboring TREM2 Missense Mutations Show Specific Deficits in Phagocytosis. *Cell Rep.* **2018**, *24*, 2300–2311. [CrossRef] [PubMed]
64. Domingues, C.; da Cruz e Silva, O.A.B.; Henriques, A.G. Impact of Cytokines and Chemokines on Alzheimer's Disease Neuropathological Hallmarks. *Curr. Alzheimer Res.* **2017**, *14*, 870–882. [CrossRef] [PubMed]
65. Doyle, K.M.; Kennedy, D.; Gorman, A.M.; Gupta, S.; Healy, S.J.M.; Samali, A. Unfolded proteins and endoplasmic reticulum stress in neurodegenerative disorders. *J. Cell. Mol. Med.* **2011**, *15*, 2025–2039. [CrossRef]
66. Cheng-Hathaway, P.J.; Reed-Geaghan, E.G.; Jay, T.R.; Casali, B.T.; Bemiller, S.M.; Puntambekar, S.S.; von Saucken, V.E.; Williams, R.Y.; Karlo, J.C.; Moutinho, M.; et al. The Trem2 R47H variant confers loss-of-function-like phenotypes in Alzheimer's disease. *Mol. Neurodegener.* **2018**, *13*, 29. [CrossRef]
67. Sudom, A.; Talreja, S.; Danao, J.; Bragg, E.; Kegel, R.; Min, X.; Richardson, J.; Zhang, Z.; Sharkov, N.; Marcora, E.; et al. Molecular basis for the loss-of-function effects of the Alzheimer's disease-associated R47H variant of the immune receptor TREM2. *J. Biol. Chem.* **2018**, *293*, 12634–12646. [CrossRef]
68. Xiang, X.; Piers, T.M.; Wefers, B.; Zhu, K.; Mallach, A.; Brunner, B.; Kleinberger, G.; Song, W.; Colonna, M.; Herms, J.; et al. The Trem2 R47H Alzheimer's risk variant impairs splicing and reduces Trem2 mRNA and protein in mice but not in humans. *Mol. Neurodegener.* **2018**, *13*, 49. [CrossRef]
69. Stomrud, E.; Björkqvist, M.; Janciauskiene, S.; Minthon, L.; Hansson, O. Alterations of matrix metalloproteinases in the healthy elderly with increased risk of prodromal Alzheimer's disease. *Alzheimers. Res. Ther.* **2010**, *2*, 20. [CrossRef]
70. Shah, K.; Desilva, S.; Abbruscato, T. The role of glucose transporters in brain disease: Diabetes and Alzheimer's Disease. *Int. J. Mol. Sci.* **2012**, *13*, 12629–12655. [CrossRef]
71. Katsel, P.; Roussos, P.; Beeri, M.S.; Gama-Sosa, M.A.; Gandy, S.; Khan, S.; Haroutunian, V. Parahippocampal gyrus expression of endothelial and insulin receptor signaling pathway genes is modulated by Alzheimer's disease and normalized by treatment with anti-diabetic agents. *PLoS ONE* **2018**, *13*, e0206547. [CrossRef]
72. Kondo, T.; Asai, M.; Tsukita, K.; Kutoku, Y.; Ohsawa, Y.; Sunada, Y.; Imamura, K.; Egawa, N.; Yahata, N.; Okita, K.; et al. Cell Stem Cell Modeling Alzheimer's Disease with iPSCs Reveals Stress Phenotypes Associated with Intracellular Ab and Differential Drug Responsiveness. *Cell Stem Cell* **2013**, *12*, 487–496. [CrossRef] [PubMed]
73. Wada, Y.; Ishiguro, K.; Itoh, T.J.; Uchida, T.; Hotani, H.; Saito, T.; Kishimoto, T.; Hisanaga, S. Microtubule-stimulated phosphorylation of tau at Ser202 and Thr205 by cdk5 decreases its microtubule nucleation activity. *J. Biochem.* **1998**, *124*, 738–746. [CrossRef] [PubMed]
74. Cruchaga, C.; Kauwe, J.S.K.; Harari, O.; Jin, S.C.; Cai, Y.; Karch, C.M.; Benitez, B.A.; Jeng, A.T.; Skorupa, T.; Carrell, D.; et al. GWAS of Cerebrospinal Fluid Tau Levels Identifies Risk Variants for Alzheimer's Disease. *Neuron* **2013**, *78*, 256–268. [CrossRef] [PubMed]
75. Piers, T.M.; Cosker, K.; Mallach, A.; Johnson, G.T.; Guerreiro, R.; Hardy, J.; Pocock, J.M. A locked immunometabolic switch underlies TREM2 R47H loss of function in human iPSC-derived microglia. *FASEB J.* **2020**, *34*, 2436–2450. [CrossRef] [PubMed]
76. Schetters, S.T.T.; Gomez-Nicola, D.; Garcia-Vallejo, J.J.; Van Kooyk, Y. Neuroinflammation: Microglia and T Cells Get Ready to Tango. *Front. Immunol.* **2017**, *8*, 1905. [CrossRef] [PubMed]

77. Duus, K.; Hansen, P.R.; Houen, G. Interaction of calreticulin with amyloid beta peptide 1-42. *Protein Pept. Lett.* **2008**, *15*, 103–107.
78. Lin, Q.; Cao, Y.; Gao, J. Serum Calreticulin Is a Negative Biomarker in Patients with Alzheimer's Disease. *Int. J. Mol. Sci.* **2014**, *15*, 21740–21753. [CrossRef]
79. Hondius, D.C.; van Nierop, P.; Li, K.W.; Hoozemans, J.J.M.; van der Schors, R.C.; van Haastert, E.S.; van der Vies, S.M.; Rozemuller, A.J.M.; Smit, A.B. Profiling the human hippocampal proteome at all pathologic stages of Alzheimer's disease. *Alzheimer's Dement.* **2016**, *12*, 654–668. [CrossRef]
80. Armstrong, A.; Mattsson, N.; Appelqvist, H.; Janefjord, C.; Sandin, L.; Agholme, L.; Olsson, B.; Svensson, S.; Blennow, K.; Zetterberg, H.; et al. Lysosomal network proteins as potential novel CSF biomarkers for Alzheimer's disease. *Neuromolecular Med.* **2014**, *16*, 150–160. [CrossRef]
81. Mody, N.; Agouni, A.; Mcilroy, G.D.; Platt, B.; Delibegovic, M. Susceptibility to diet-induced obesity and glucose intolerance in the APP SWE/PSEN1 A246E mouse model of Alzheimer's disease is associated with increased brain levels of protein tyrosine phosphatase 1B (PTP1B) and retinol-binding protein 4 (RBP4), and basal phosphorylation of S6 ribosomal protein. *Diabetologia* **2011**, *54*, 2143–2151. [CrossRef]
82. Bonham, L.W.; Geier, E.G.; Steele, N.Z.R.; Holland, D.; Miller, B.L.; Dale, A.M.; Desikan, R.S.; Yokoyama, J.S.; Initiative, A.D.N. Insulin-Like Growth Factor Binding Protein 2 Is Associated With Biomarkers of Alzheimer's Disease Pathology and Shows Differential Expression in Transgenic Mice. *Front. Neurosci.* **2018**, *12*, 476. [CrossRef] [PubMed]
83. Katayama, T.; Imaizumi, K.; Sato, N.; Miyoshi, K.; Kudo, T.; Hitomi, J.; Morihara, T.; Yoneda, T.; Gomi, F.; Mori, Y.; et al. Presenilin-1 mutations downregulate the signalling pathway of the unfolded-protein response. *Nat. Cell Biol.* **1999**, *1*, 479–485. [CrossRef] [PubMed]
84. Hamos, J.E.; Oblas, B.; Pulaski-Salo, D.; Welch, W.J.; Bole, D.G.; Drachman, D.A. Expression of heat shock proteins in Alzheimer's disease. *Neurology* **1991**, *41*, 345–350. [CrossRef] [PubMed]
85. Hoozemans, J.J.M.; Veerhuis, R.; Van Haastert, E.S.; Rozemuller, J.M.; Baas, F.; Eikelenboom, P.; Scheper, W. The unfolded protein response is activated in Alzheimer's disease. *Acta Neuropathol.* **2005**, *110*, 165–172. [CrossRef]
86. Han, J.; Back, S.H.; Hur, J.; Lin, Y.-H.; Gildersleeve, R.; Shan, J.; Yuan, C.L.; Krokowski, D.; Wang, S.; Hatzoglou, M.; et al. ER-stress-induced transcriptional regulation increases protein synthesis leading to cell death. *Nat. Cell Biol.* **2013**, *15*, 481–490. [CrossRef]
87. Kim, D.; Langmead, B.; Salzberg, S.L. HISAT: A fast spliced aligner with low memory requirements. *Nat. Methods* **2015**, *12*, 357–360. [CrossRef]
88. Baruzzo, G.; Hayer, K.E.; Kim, E.J.; Di Camillo, B.; FitzGerald, G.A.; Grant, G.R. Simulation-based comprehensive benchmarking of RNA-seq aligners. *Nat. Methods* **2017**, *14*, 135–139. [CrossRef]
89. Li, H.; Handsaker, B.; Wysoker, A.; Fennell, T.; Ruan, J.; Homer, N.; Marth, G.; Abecasis, G.; Durbin, R. The Sequence Alignment/Map format and SAMtools. *Bioinformatics* **2009**, *25*, 2078–2079. [CrossRef]
90. Liao, Y.; Smyth, G.K.; Shi, W. featureCounts: An efficient general purpose program for assigning sequence reads to genomic features. *Bioinformatics* **2014**, *30*, 923–930. [CrossRef]
91. Law, C.W.; Chen, Y.; Shi, W.; Smyth, G.K. Voom: Precision weights unlock linear model analysis tools for RNA-seq read counts. *Genome Biol.* **2014**, *15*, R29. [CrossRef]
92. Smyth, G.K. Linear Models and Empirical Bayes Methods for Assessing Differential Expression in Microarray Experiments. *Stat. Appl. Genet. Mol. Biol.* **2004**, *3*. [CrossRef] [PubMed]
93. Gentleman, R.C.; Carey, V.J.; Bates, D.M.; Bolstad, B.; Dettling, M.; Dudoit, S.; Ellis, B.; Gautier, L.; Ge, Y.; Gentry, J.; et al. Bioconductor: Open software development for computational biology and bioinformatics. *Genome Biol.* **2004**, *5*, R80. [CrossRef] [PubMed]
94. Gautier, L.; Cope, L.; Bolstad, B.M.; Irizarry, R.A. affy-analysis of Affymetrix GeneChip data at the probe level. *Bioinformatics* **2004**, *20*, 307–315. [CrossRef] [PubMed]
95. Warnes, G.R.; Bolker, B.; Bonebakker, L.; Gentleman, R.; Liaw, W.H.A.; Lumley, T.; Maechler, M.; Magnusson, A.; Moeller, S.; Schwartz, M.; et al. gplots: Various R Programming Tools for Plotting Data. *R Package Version* **2015**.
96. Chen, H.; Boutros, P.C. VennDiagram: A package for the generation of highly-customizable Venn and Euler diagrams in R. *BMC Bioinf.* **2011**, *12*, 35. [CrossRef] [PubMed]

97. Graffmann, N.; Ring, S.; Kawala, M.-A.; Wruck, W.; Ncube, A.; Trompeter, H.-I.; Adjaye, J. Modeling Nonalcoholic Fatty Liver Disease with Human Pluripotent Stem Cell-Derived Immature Hepatocyte-Like Cells Reveals Activation of PLIN2 and Confirms Regulatory Functions of Peroxisome Proliferator-Activated Receptor Alpha. *Stem Cells Dev.* **2016**, *25*, 1119–1133. [CrossRef]
98. Chatr-aryamontri, A.; Oughtred, R.; Boucher, L.; Rust, J.; Chang, C.; Kolas, N.K.; O'Donnell, L.; Oster, S.; Theesfeld, C.; Sellam, A.; et al. The BioGRID interaction database: 2017 update. *Nucleic Acids Res.* **2017**, *45*, D369–D379. [CrossRef]
99. Csardi, G.; Nepusz, T. The igraph software package for complex network research. *InterJournal* **2006**, *1695*, 1–9.
100. Butts, C. network: A Package for Managing Relational Data in R. *J. Stat. Softw.* **2008**, *24*, 2. [CrossRef]
101. Kanehisa, M.; Furumichi, M.; Tanabe, M.; Sato, Y.; Morishima, K. KEGG: New perspectives on genomes, pathways, diseases and drugs. *Nucleic Acids Res.* **2017**, *45*, D353–D361. [CrossRef]
102. Falcon, S.; Gentleman, R. Using GOstats to test gene lists for GO term association. *Bioinformatics* **2007**, *23*, 257–258. [CrossRef] [PubMed]